AADE-11-NTCE-45



Effect of Rotation on Flowrate and Pressure Gradient in Eccentric Holes

Wilson Chin and Xiaoying Zhuang, Stratamagnetic Software, LLC

Copyright 2011, AADE

This paper was prepared for presentation at the 2011 AADE National Technical Conference and Exhibition held at the Hilton Houston North Hotel, Houston, Texas, April 12-14, 2011. This conference was sponsored by the American Association of Drilling Engineers. The information presented in this paper does not reflect any position, claim or endorsement made or implied by the American Association of Drilling Engineers, their officers or members. Questions concerning the content of this paper should be directed to the individual(s) listed as author(s) of this work.

Abstract

In pre-1990s literature, exact non-Newtonian flow solutions and field experiences consistently demonstrated that drillstring rotation increases flowrate for a fixed pressure gradient, or equivalently, decreases pressure gradient (magnitude) for a fixed flowrate, the effect being attributed to apparent viscosity reduction due to shear-thinning. Field experiences in the past two decades, however, indicate the exact opposite, and recent papers have failed to determine the causes of the apparent contradictions and resulting confusion. It turns out that there are no inconsistencies: the boreholes considered recently are highly eccentric because they are deviated or horizontal, for which new convective terms in the governing momentum equations appear which are due to annular eccentricity and which modify the effective pressure gradient (these terms are not present in older studies, which consider only concentric annuli). Exact numerical solutions demonstrate the role of eccentricity in changing flowrate or pressure gradient during drilling. Because the changes are not small, drillstring rotation can be used to control pressure in managed pressure drilling applications and in cementing. The implications are more efficient drilling and improved safety. The computational model developed uses boundaryconforming, curvilinear mesh systems to describe annular geometry exactly, and rapidly converging, stable, transient algorithms have been developed to solve the general rheology equations with and without yield stresses.

Introduction

Non-Newtonian flows in highly eccentric annuli with cuttings beds, washouts and fractures, encountered in cementing and managed pressure (and underbalanced) drilling, are solved without crude slot flow and hydraulic radius approximations. The nonlinear partial differential equations, written to customized, boundary-conforming, curvilinear coordinate grid systems providing high physical resolution in tight spaces, are solved exactly with no-slip conditions, and detailed velocity, apparent viscosity, shear rate and viscous stress fields are computed for pressure drop, hole cleaning and other applications. For fluids with yield stress, well known uncertainties related to plug zone size and shape are fully resolved using Herschel-Bulkley relations applicable across transition boundaries (determined iteratively as part of the solution) reaching into and across the plug. Two-dimensional, single-phase, steady flow simulations, solved rapidly using finite difference methods, provide detailed numbers and color displays for all physical quantities within seconds, with excellent numerical stability for all fluid types with and without yield stress. Formulations for steady-state casing or drillpipe longitudinal translation and rotation are presented, and extensions to model transient incompressible effects associated with starting, stopping and periodic movement, important in evaluating cement-mud displacement efficiency, axial-helical cuttings transport, swab-surge, and jarring remedies for freeing stuck pipe, are developed. Practical problems are presented and the advantages over existing models are described.

In this paper, extensive calculation methods and new modeling capabilities are presented for job planning and steady-state and fully transient rotating flow analysis in modern managed pressure drilling applications.

Background

Annular flow modeling in boreholes, important to both drilling and cementing, is as old as petroleum engineering itself. In the simplest case, flow configurations are represented by concentric circles through which steady, two-dimensional, Newtonian and power law fluids flow; in these limits, exact analytical or numerical solutions of the flow equations provide useful tools for operational applications. For more complicated problems, e.g., eccentric annuli, non-ideal geometric irregularities, non-Newtonian yield stress fluids, pipe translation and rotation, however, numerous mathematical obstacles arise, which unfortunately introduce inefficiencies into field practices. We discuss these problems next.

Geometric complications. In deviated and horizontal wells, heavy pipe and drill collar weight implies eccentric positioning within the borehole, as shown in (a) of Fig. 1, leading to difficulties in geometric description and solution. High eccentricities are often accompanied by non-symmetrical washouts, thick and irregularly formed cuttings beds, and possibly, fracture indentations. Early in petroleum engineering, the notion of a simple "mean hydraulic radius" permitting representation as an equivalent circular pipe flow, as depicted in (b) of Fig. 1, was widely employed; this approach, however, was not useful since what is meant by "mean" is not obvious and certainly not generally applicable from one situation to the next. Later "slot flow" models "unwrapped" the eccentric annulus, with the result as

illustrated in (c) of Fig. 1, and then, further discretized the resulting slot into local parallel plate elements, each of which is approximately modeled by simple solutions for fluid flow between ideal parallel plates. While somewhat reasonable, this approach applied strictly to very narrow annuli, but even then, curvature terms in the general governing momentum equations are always neglected. Thus, inertial effects are never properly modeled even in the limit of very narrow elements.

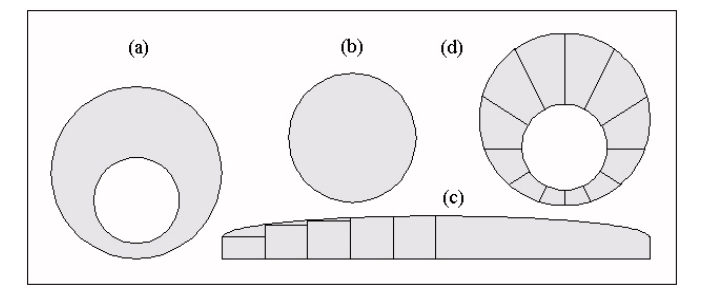


Fig. 1 – Idealizations commonly used to represent eccentric borehole annuli.

Improvements to slot flow models are provided by "pie slice" formulations, idealized in (d) of Fig. 1, in which eccentric annuli are represented by "pie slices" of varying size and included angle having the pipe center as a virtual origin. The solution for each slice is taken from the numerical solution for a concentric annular problem with a closely matched radius. In this approach, pie slices ranging from small to large are used. However, it is clear from the sketch that perfect geometric matching of the borehole boundary is never completely achieved, so that adequate modeling of curvature effects is approximate at best. Moreover, the concentric solutions used are numerical in the case of yield stress fluids and awkward in implementation. More recently, authors have used "bipolar coordinates" to represent eccentric circles, and while these provide useful host formulations for zero-yield-stress fluids, the algebra required to represent even the simplest non-Newtonian flow problems is overwhelming compared to the methods introduced later. The mapping method used in the present paper, it turns out, provides superior modeling capabilities in that the complete momentum equation for any rheology and annular geometry can be solved exactly. The new approach is less intensive numerically and easily describes realistic cuttings beds, washouts and fracture indentations.

Geometric difficulties, however, are much more than what meets the eye. When yield stress fluids flow, "plug regimes" that move as solid bodies are always present in flow domains below a given yield stress. When slot flow or pie slice models are used to simplify the solution process, "plug rings" are always obtained by virtue of the adhoc recipes described above. This is physically incorrect in most operational situations characterized by high eccentricity. For example, one would expect a large, isolated, almost circular plug element at the wide side of (a) of Fig. 1 and perhaps in a narrow strip at the bottom, but a flow containing such a solid

plug would be ruled out by both solution methods. Until recently, of course, exact solutions for (a) Fig. 1 with yield stress fluids, e.g., Bingham plastics and Herschel-Bulkley models, were impossible anyway for one important reason – theoretically, the size and shape of the plug zone are unknown in problems without azimuthal symmetry, and without knowledge of these internal boundary properties, a complete flow solution could not be obtained. This paper addresses and solves this problem in its complete generality.

Mathematical difficulties. Ideally, one would represent the details of highly eccentric annular domains exactly and in their entirety using boundary-conforming, curvilinear meshes, to which the governing equations of motion would be written, solved, and post-processed for relevant engineering information. However, this is often numerically difficult because there are as many distinct partial differential equation formulations as there are fluid rheologies, e.g., the equations for Newtonian, power law, Bingham plastic and Herschel-Bulkley fluids are very different, each with its own convergence, stability and physical properties. Moreover. because the equations are generally nonlinear, solutions must be obtained by iterative means. In fact, iterative solutions solving complicated grid generation equations must be followed by iterative solutions to produce the required flowfields on the resulting meshes. These difficulties are compounded, typically, by user inexperience in computational grid generation and numerical analysis. Even when solutions to underlying velocity fields are available, post-processed field solutions for shear rate, viscous stress, apparent viscosity, and so on, need to be automated and rapidly displayed in order to be useful in real-time applications. This requirement is particularly relevant in ultra-deepwater applications since fast and accurate pressure solutions are required to navigate the narrow window between formation fracture and disastrous blowout. These problems are all addressed in the software development program.

User interface considerations. Assuming that both geometric and mathematical issues can be addressed satisfactorily, human factors issues relating to software usage become all-important especially in the anticipated applications to managed pressure drilling in ultra-deepwater drilling and hole-cleaning at high deviation angles. Physical formulations must be mathematically rigorous, numerical solutions must be detailed and pertinent to the annular geometry at hand, and complete field solutions for all engineering properties must be achievable in a manner that is completely transparent to typical engineering users with undergraduate degrees – and, even better, to field technicians with minimal modeling experience or mathematical training. This requires fully automatic grid generation, nonlinear equation setup and stable matrix inversion.

The user interface must be designed with rigsite workflows in mind. Importantly, accuracy and speed, that is, "desktop speed" from problem definition to automated color displays, go hand-in-hand, because of demands imposed by narrow margins between pore-pressure and fracture-pressure gradient profiles in modern offshore applications. All of the

above considerations, again, accurate geometric modeling, rigorous mathematical formulation and solution, and fast, user-friendly, graphically-oriented software implementation, render the general annular flow modeling problem extremely challenging. We now address each of the foregoing issues and explain how the solutions satisfactorily address these needs.

Exact Geometric and Mathematical Formulation

Boundary-conforming, curvilinear meshes. Coordinate systems "natural" to engineering problems play vital roles in facilitating efficient and accurate computational solutions. For example, circular coordinates are natural to circular wells producing from infinite reservoirs, while rectangular systems are ideal for problems solving, say, temperature distributions on rectangular plates. By the same token, a mesh system suitable for eccentric annular geometries would have inside coordinate lines that coincide with circular or square drill collars with stabilizers, while outside lines would conform to irregular borehole walls with their cuttings beds, washouts and fracture indentations. A second set of coordinate lines might be constructed orthogonally to the first, although this is not necessary if all terms in the resulting transformed governing equations are retained. By contrast, it is clear that rectangular (x,y) or circular (r,θ) coordinates are less than satisfactory for accurate geometric description of general annuli.

In natural "boundary-conforming, curvilinear coordinates," here denoted by (ξ,η) , boundary conditions would be easily specified. For example, the no-slip velocity condition for stationary surfaces, say, at pipe and borehole surfaces, is simply described by "u=0" along horizontal grid lines $\xi=\xi_{\text{pipe}}$ and $\xi=\xi_{\text{borehole}}$ where the subscripted numbers are constants. By contrast, the formulation in rectangular coordinates would require u=0 applied along cumbersome curves, e.g., $u\{x,f(x)\}=0$ where y=f(x) represents internal and external contours.

The objective behind grid generation is a set of transformations $\xi(x,y)$ and $\eta(x,y)$ that enable simple boundary condition implementation, so that a complicated physical region, here the eccentric borehole annulus, becomes a simple rectangular one in a computational domain, where the solution of the mathematical problem is undertaken. Once the mapping transforms are available, the governing equation itself must be expressed in the new coordinates. For example, the partial differential equation for steady-state, two-dimensional, Newtonian fluid flow is the well known $u_{xx} + u_{yy} = -\mu^{-1} \frac{\partial P}{\partial z}$ where μ and $\frac{\partial P}{\partial z}$ represent viscosity and applied pressure gradient. Although this appears in rectangular coordinates, the equation applies to all annular geometries.

The conversion process itself is straightforward. Suppose we wish to express a function u(x,y) in terms of convenient independent variables ξ and η . If the transformations $x=x(\xi,\eta)$ and $y=y(\xi,\eta)$ are available, direct substitution allows us to rewrite u(x,y) in the form $u(x,y)=U(\xi,\eta)$, where the functional relation $U(\xi,\eta)$ between ξ and η is generally different from the relation u(x,y) connecting x

and y. Derivatives of u(x,y) with respect to x and y are easily related to derivatives of $U(\xi,\eta)$ taken with respect to ξ and η . For example, it is easily shown that $U_\xi = u_x x_\xi + u_y \ y_\xi$ and $U_\eta = u_x x_\eta + u_y \ y_\eta$ for the first derivatives, with obvious extensions to second derivatives obtained using the chain rule of calculus. In general fluid-dynamical problems, the resulting equation for $U(\xi,\eta)$ is typically more complicated than that for u(x,y). The computational benefit, however, is accurate and noise-free implementation of boundary conditions, not to mention the use of much fewer grid points for the same level of physical resolution. Calculated solutions are displayed in physical space with the assistance of custom color plotting routines.

Many commercial simulators calculate velocities and other flow properties directly using rectangular (x,y) grids. We emphasize that x-y coordinate lines do not conform to the irregular curves defining near and farfield boundaries; also, high grid densities imposed, say at the bottom of an eccentric annulus, would require similarly high densities far away where detailed resolution is unnecessary. This results in large, inefficient computing domains containing dead flow and extremely large matrices. In addition, "choppy" meshes lead to noise, inaccuracy and instability. Other simulators, particularly general purpose codes used in computational fluid dynamics (CFD), do support automatic and efficient "finite element" or "finite volume" gridding. However, they are not portable in the sense that special licenses must be purchased for users, thus incurring significant costs. importantly, they run proprietary, high-overhead "canned" routines that cannot be adapted to new mathematical models (such as the novel yield stress formulation introduced below) and cannot be "tuned" to run optimally. Also, they offer inflexible output formats that are not easily integrated with custom designed graphics and user interface software. In this paper, the objective is a fast, flexible and accurate solution procedure that can be installed on all operating systems at minimal cost.

We conceptually describe the grid generation process in this paper. Details are offered in the principal author's books on drilling and reservoir engineering, e.g., see Chin (1992, 2001, 2002). We reiterate the basic ideas here because they are essential to understanding the solution approach and its topological advantages. Rather than dealing directly with $\xi = \xi(x,y)$ and $\eta = \eta(x,y)$, we equivalently consider the inverse functions $x = x(\xi,\eta)$ and $y = y(\xi,\eta)$ satisfying *nonlinear* coupled partial differential equations, which are derived in the form

$$\begin{array}{l} (x_{\eta}^{\; 2} + y_{\eta}^{\; 2}) \; x_{\xi\xi} \; - 2 \; (x_{\xi}x_{\eta} + y_{\xi}y_{\eta}) \; x_{\xi\eta} \; + (x_{\xi}^{\; 2} + y_{\xi}^{\; 2}) \; x_{\eta\eta} \; = 0 \quad (1) \\ (x_{\eta}^{\; 2} + y_{\eta}^{\; 2}) \; y_{\xi\xi} \; - 2 \; (x_{\xi}x_{\eta} + y_{\xi}y_{\eta}) \; y_{\xi\eta} \; + (x_{\xi}^{\; 2} + y_{\xi}^{\; 2}) \; y_{\eta\eta} \; = 0 \quad (2) \end{array}$$

where ξ and η are now independent (as opposed to dependent) variables. We aim to map the irregular flow domain of Fig. 2a into the simple rectangular computational domain of Fig. 2b where B_1 and B_2 are physically insignificant "branch cuts" where single-valued solution constraints are enforced.

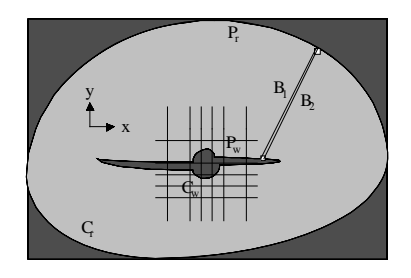


Fig. 2a – Irregular physical domain with inefficient rectangular meshes.

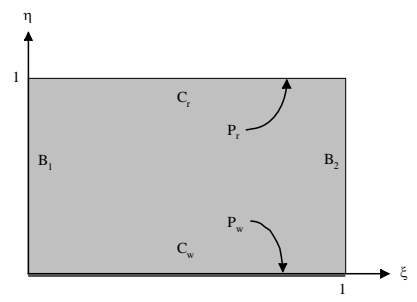


Fig. 2b – Irregular domain mapped to rectangular computational space.

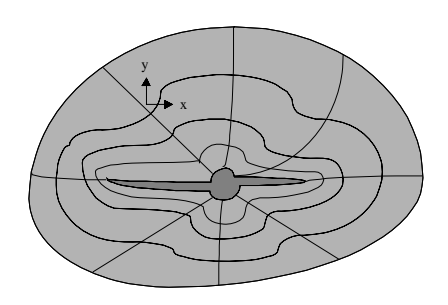


Fig. 2c - Physical domain in boundary-conforming coordinates.

How are the foregoing equations used to create numerical mappings? Suppose that contour C_W in Fig. 2a is to map into $\eta=0$ of Fig. 2b. The user first discretizes C_W in Fig. 2a by penciling along it a sequence of dots chosen to represent the curve. If these are selected in an orderly, say, clockwise fashion, they define the direction in which ξ increases. Along $\eta=0$, values of x and y are known (e.g., from measurement on graph paper) as functions of ξ . Similarly, x and y values along C_r are known as functions of ξ on $\eta=1$ of Fig. 2b. These provide the boundary conditions for Eqs. 1 and 2, which are augmented by single-valuedness constraints at arbitrarily chosen branch cuts B_1 and B_2 . It is clear that this process is easily automated by computer.

Conventionally, in grid generation, Eqs. 1 and 2 are discretized by finite differences and solved by point or line relaxation, starting with guesses for the dependent variables x and y. The problem is linearized by approximating all nonlinear coefficients using values from earlier iterations. Typically, several updates to Eq. 1 are taken, followed by updates to Eq. 2, with this cycling process, often unstable, repeated continuously until convergence. Variations of the

approach are known, with 100×100 mesh systems in the ξ - η plane requiring minutes of computing time. Once $x = x(\xi,\eta)$ and $y = y(\xi,\eta)$ are solved and tabulated as functions of ξ and η , physical coordinates are generated. First, η is fixed; for each node ξ along this η , computed values of (x,y) pairs are successively plotted in the x-y plane to produce the required closed contour. This procedure is repeated for all values of η , until the entire family of closed curves is obtained, with limit values $\eta = 0$ and $\eta = 1$ again describing C_w and C_r . Orthogonals are constructed by repeating the procedure, with η and ξ roles reversed.

This process provides the curvilinear mapping only. The equation describing the physics (e.g., the Navier-Stokes equation for Newtonian flow or the general rheological equations for non-Newtonian fluids) must be transformed into (ξ,η) coordinates and solved. In general, the transformed governing equation, which is algebraically more complicated, must be solved, and this procedure introduces its own complications and numerical challenges. "simplification," however, lies not in the transformed equation, which now contains mixed derivatives and variable coefficients, but in the computational domain itself, because this domain takes on a rectangular form amenable to simple, noise-free numerical solution, requiring significantly fewer nodal points for high resolution physical definition.

Again, existing solution methods solving $x(\xi,\eta)$ and $y(\xi,\eta)$ stagger the solutions for Eqs. 1 and 2. For example, crude solutions are used to initialize the coefficients of Eq. 1, and improvements to $x(\xi,\eta)$ are obtained. These are used to evaluate the coefficients of Eq. 2, in order to obtain an improved $y(\xi,\eta)$; then, attention turns to Eq. 1 again, and so on, until convergence is achieved. Various over-relaxation means are used to implement these iterations, e.g., point SOR, line SLOR, line SOR with explicit damping, alternatingdirection-implicit, and multigrid, with varying degrees of success. Often these schemes diverge computationally. In any event, the staggering used introduces different artificial Classic numerical analysis, time levels while iterating. however, suggests that faster convergence and improved stability are possible by reducing the number of time levels.

A new approach to rapidly solve the nonlinear coupled grid generation equations was proposed by the principal author a decade ago and is based on a very simple idea. This idea has since been validated in numerous applications. Consider first $z_{\xi\xi}+z_{\eta\eta}=0,$ for which $z_{i,j}\approx(z_{i-1,j}+z_{i+1,j}+z_{i,j-1}+z_{i,j+1})/4$ holds on constant grid systems (this is easily derived using standard finite difference formulas). This well-known averaging law motivates the $\mathit{recursion formula}\ z_{i,j}^n=(z_{i-1,j}^{n-1}+z_{i+1,j}^{n-1}+z_{i,j-1}^{n-1}+z_{i,j+1}^{n-1})/4$ often used to illustrate and develop multilevel iterative solutions; an approximate, and even trivial solution, can be used to initialize the calculations, and nonzero solutions are always produced from nonzero boundary conditions.

But the well-known Gauss-Seidel method is fastest: as soon as a new value of $z_{i,j}$ is calculated, its previous value is discarded and overwritten by the new value. This speed is

accompanied by low memory requirements, since there is no need to store both n and n-1 level solutions: only a single array, $z_{i,j}$ itself, is required in programming. The approach to Eqs. 1 and 2 was motivated by the following idea. Rather than solving for $x(\xi,\eta)$ and $y(\xi,\eta)$ in a staggered, leap-frog manner, is it possible to $\emph{simultaneously}$ update x and y in a similar once-only manner? Are convergence rates significantly increased? What formalism permits us to solve in Gauss-Seidel fashion? What are the programming implications?

Complex variables are used often in harmonic analysis problems; for example, the real and imaginary parts of an analytical function f(z), where z=x+i y, provide solutions satisfying Laplace's equation. Here we use complex analysis differently. We *define* a dependent variable z by $z(\xi,\eta)=x(\xi,\eta)+i$ y(ξ,η), and then add Eq. 1 plus i times Eq. 2, in order to obtain the net result $(x_{\eta}^2+y_{\eta}^2)$ $z_{\xi\xi}-2$ $(x_{\xi}x_{\eta}+y_{\xi}y_{\eta})$ $z_{\xi\eta}+(x_{\xi}^2+y_{\xi}^2)$ $z_{\eta\eta}=0$. Now, the complex conjugate of z is $z'(\xi,\eta)=x(\xi,\eta)-i$ y(ξ,η), from which we find that $x=(z+z^*)/2$ and y=-i ($z-z^*$)/2. Substitution produces the simple and equivalent one-equation result

$$(z_{\eta}\,z_{\eta}^{\,\,*})\,z_{\xi\xi}\,\text{-}\,(z_{\xi}\,z_{\eta}^{\,\,*}+z_{\xi}^{\,\,*}z_{\eta}^{\,\,})\,z_{\xi\eta}^{\,\,}+(z_{\xi}\,z_{\xi}^{\,\,*})\,z_{\eta\eta}^{\,\,}=0\ (3)$$

This form yields significant advantages. First, when z is declared as a complex variable in a Fortran program, Eq. 3 represents, for all practical purposes, a single equation in $z(\xi,\eta)$. There is no need to leap-frog between x and y solutions now, since a single formula analogous to the classical model $z_{i,j}=(z_{i-1,j}+z_{i+1,j}+z_{i,j-1}+z_{i,j+1})/4$ is easily written for the $z_{i,j}$ using Eq. 3 as the host equation. Because both x and y are simultaneously resident in computer memory, the extra time level present in staggered schemes is completely eliminated, as in the Gauss-Seidel method. In thousands of test simulations conducted using point and line relaxation, convergence times are shorter by orders of magnitude relative to those obtained for cyclic solution between $x(\xi,\eta)$ and $y(\xi,\eta)$. Convergence appears to be unconditional, monotonic and stable. Because Eq. 3 is nonlinear, von Neumann tests for exponential stability and traditional estimates for convergence rate do not apply, but the evidence for stability and convergence, while empirical, remains very strong and convincing since we have always computed useful grids in all test runs.

Iterative solution of nonlinear partial differential equations. Earlier we noted that $u_{xx} + u_{yy} = -\mu^{-1} \partial P/\partial z$ applies to steady, two-dimensional, single-phase Newtonian flows for borehole annuli having the most complicated shapes; unfortunately, practical solutions cannot be accurately obtained in (x,y) coordinates. Here, μ is a constant viscosity and $\partial P/\partial z$ is the applied pressure gradient in the z direction assumed to be known. This is the so-called Poisson equation in mathematics, and students who have undertaken its study realize that, despite the apparent simplicity offered by few terms and complete linearity, useful solutions to the classical model are nonetheless difficult to obtain. When the underlying fluid is nonlinear, this equation is replaced by Eq. 4, which is vastly more complicated, that is,

$$\partial (N \partial u/\partial y)/\partial y + \partial (N \partial u/\partial x)/\partial x = \partial P/\partial z$$
 (4)

where N now represents the "apparent viscosity" function. This apparent viscosity is not constant, but a function of local shear rates whose mathematical form depends on the particular rheology assumed. For example, in the case of power law fluids modeled by an exponent "n" and a consistency factor "K," N takes the form $N = K \left[(\partial u/\partial y)^2 + (\partial u/\partial x)^2 \right]^{(n-1)/2}$. Even without solving the problem, it is clear that, since $\partial u/\partial x$ and $\partial u/\partial y$ depend on the (unknown) solution itself, any resulting apparent viscosity must vary locally within the flow domain and depend on both geometric details and flow rate. Detailed computed solutions for annular flows are presented in Chin (1992, 2001) where approximate approaches to plug flow modeling are used.

Because Eq. 4 is now strongly nonlinear, the solution process at its very heart must remain nonlinear. This implies that one cannot use simpler Newtonian solutions as leading approximations and focus on higher order improvements to them. The basic solution method must retain a fully nonlinear character in order that well known nonlinear relationships between pressure gradient and volume flow rate evolve as part of an iterative computational process. As if this alone were not complicated enough, we emphasize that it is the reexpression of Eq. 4 in general (ξ,η) curvilinear coordinates, not in simple (x,y) coordinates, that must be solved, and that these coordinates and their metrics are only available numerically.

The transformed equation now contains additional terms as well as nonlinear coefficients that depend on the mapping. Direct solutions are not numerically possible, but exact solutions can be obtained iteratively. In fact, finite difference methods are used; the solutions are obtained line-by-line using so-called "successive line over relaxation" (SLOR) schemes written in the curvilinear coordinates. These iterative solutions are initialized by "close" analytical or numerical solutions; the closer the initial guess, the more rapid the convergence. For typical problems, the efficient schemes devised will produce a usable curvilinear grid in approximately one second of computing time, while the solution of the transformed momentum equation (when pressure gradient is specified) may require two-to-three seconds. Again, detailed discussions and computed solutions for power law and simple plug flows in highly eccentric annuli, with practical applications, are given in Chin (1992, 2001). The approximate plug flow methods developed in these early researches are now obsolete and are replaced by the following exact approach for yield stress description and

Yield stress, plug zone size and shape modeling. In fluid flows where yield stresses exist, "plug zones" are to be found. These plugs move as solid bodies within the flowing system. For pipes with circular cross-sections and for concentric annuli, it is possible to derive exact analytical solutions for plug zone size and shape for Bingham plastics (general solutions have, in fact, been derived for both

geometries assuming Herschel-Bulkley fluids, and will be presented separately). For circular pipes, the cross-sectional plug is simply a circle; for concentric annuli, of course, the plug is a concentric ring.

The appearance of solid plugs within moving streams results from the rheological model used by mathematicians to idealize the physics. If we denote the shear rate functional by $\Gamma = [\ (\partial u/\partial y)^2 + (\partial u/\partial x)^2\]^{1/2}, \text{ this idealization can be written formally as}$

$$\begin{split} N &= k \; \Gamma^{n-1} + S_{yield} / \Gamma \; \text{if} \; \{1/2 \; \text{trace} \; (\underline{\underline{\mathbf{S}}} \bullet \underline{\underline{\mathbf{S}}}) \}^{1/2} > \tau_0 \\ \underline{\underline{\mathbf{D}}} &= 0 \; \text{if} \; \{1/2 \; \text{trace} \; (\underline{\underline{\mathbf{S}}} \bullet \underline{\underline{\mathbf{S}}}) \}^{1/2} < \tau_0 \end{split} \tag{5}$$

where the general extra stress tensor is denoted by $\underline{\underline{S}}$ and the deformation tensor is given by $\underline{\underline{D}}$. Here, τ_0 is the so-called "yield stress." The discontinuous "if, then" character behind Eq. 5 is responsible for the sudden transition from shear flow to plug flow commonly quoted. As noted, for flows with azimuthal symmetry, that is, circular pipes and concentric annuli, exact, rigorous mathematical solutions are in fact possible.

For non-circular ducts and eccentric annuli, which describe a large number of practical engineering problems, it has not been possible to characterize plug zone size and shape, even approximately. Thus, the most significant petroleum engineering flow problems important to both drilling and cementing cannot be modeled at all, let alone accurately. In order to remedy this situation, we observe that the discontinuity offered in Eq. 5 is really an artificial one, introduced for, of all reasons, "simplicity." This unfortunately leads to the solution difficulties noted. In reality, practical engineering flows do not suddenly turn from shear to plug flow; the transition may be rapid, but it will occur continuously over finite measurable distances. We therefore turn to more realistic rheological models which apply continuously throughout the entire problem domain, and which, if the underlying flow parameters permit, lead to plug zones naturally during the solution process.

The conventional Herschel-Bulkley viscoplastic model, which includes Bingham plastics as a special limit when the exponent "n" is unity, requires that $\tau = \tau_0 + K(d\gamma/dt)^n$, if $\tau > \tau_0$ and $d\gamma/dt = 0$ otherwise. Here τ is the shear stress, τ_0 is the yield stress, K is the consistency factor, K is the exponent, and K is the shear rate. As explained, this model is far from perfect. For example, both Herschel-Bulkley and Bingham plastic models predict infinite viscosities in the limit of vanishing shear rate, a fact that often leads to numerical instabilities. In addition, the behavior is not compatible with conservation laws that govern many complex flows.

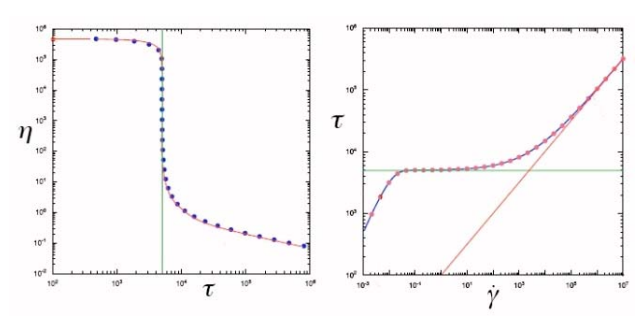


Fig. 3 - Extended Herschel-Bulkley law.

An alternative to the standard Herschel-Bulkley model is the use of continuous functions which apply to sheared regimes, and in addition, through and into the plug zone. One such example model is suggested by Souza, Mendez and Dutra (2004), that is, $\tau = \{1 - \exp(-\eta_0 \ d\gamma/dt \ /\tau_0)\}\{\tau_0 + K \ (d\gamma/dt)^n\}$, which would apply *everywhere* in the problem domain. The corresponding apparent viscosity N, for numerical implementation in Eq. 4, is denoted by

$$\begin{split} \eta &= \tau \, / (d\gamma \, / dt) \\ &= \{1 - exp(-\eta_0 \, d\gamma / dt \, / \tau_0)\} \{\tau_0 / (d\gamma / dt) + K \, (d\gamma / dt)^{n-1}\} \end{split} \tag{6}$$

The "apparent viscosity vs shear stress" and "shear stress vs shear rate" diagrams, from Souza et al, are duplicated in Fig. 3. What are the physical consequences of this model? Eq. 6, in fact, represents an "extended Herschel-Bulkley" model in the following sense. For infinite shear rates, one would recover $\tau = \tau_0 + K (d\gamma/dt)^n$. But for low shear rates, a simple Taylor expansion leads to $\eta \approx \{\eta_0(d\gamma/dt)/\tau_0\}\{\tau_0/(d\gamma/dt) + K$ $(dy/dt)^{n-1}$ $\approx \eta_0$ where it is clear now that η_0 represents a very high viscosity for the plug zone. The use of Eq. 6 in numerical algorithms simplifies both formulation and coding since internal boundaries and plug domains do not need to be determined as part of the solution. A single constitutive law (as opposed to the use of two relationships in Eq. 5) applies everywhere, thus simplifying computational logic; moreover, the continuous function assumed also possesses continuous derivatives everywhere and allows the use of standard difference formulas. Cumbersome numerical matching across internal boundaries is completely avoided. In a practical computer program, the plug zone viscosity might be assumed, for example, as 1,000 cp. In fact, we choose high values of η_0 which would additionally stabilize the numerical integration schemes used. This strategy is applied throughout this work, both to the iterative relaxation schemes for steady-state problems and to the transient integration schemes for more complicated formulations. This new approach was first discussed in Chin and Zhuang (2010) for steady flows and has since been incorporated in the fully transient annular flow modeling approaches.

Borehole axis radius of curvature. Borehole axis curvature is important to ultra-deepwater drilling, especially in short and medium radius turning applications. Several aspects of cuttings transport and debris removal are not completely understood insofar as centrifugal effects are concerned and a

study of curvature effects contributes to an understanding of their influence on stress fields. Also, bends in pipelines and annuli are interesting because they are associated with losses; that is, to maintain a prescribed volume flow rate, a greater pressure drop is required in pipes with bends than those without. This is true because the viscous stresses acting along pipe walls are higher. The modeling of borehole axis curvature effects for problems involving noncircular ducts and highly eccentric annuli containing non-Newtonian fluids was first addressed in Chin (2001), where detailed derivations, equations and computed examples are given. Essentially, it is shown how, by replacing " $1/\mu$ $\partial P/\partial z$ " with an inertially corrected " $1/\mu$ $\partial P/\partial z - 1/R$ $\partial u/\partial r + u/R^2$ " where R is the radius of curvature, the effective pressure gradient accounting for centrifugal effects is properly and stably modeled. This model is incorporated into Eq. 4 and a radius of curvature entry appears in the software menu in Fig. 4a at the bottom left.

Steady and Transient Formulations: User Interface and Physical Modeling Capabilities

Simulators for two-dimensional steady and transient flow are described in this paper, applicable to single-phase, Herschel-Bulkley fluids, which may also be operated in Newtonian, power law and Bingham plastic modes. For Bingham plastic and Herschel-Bulkley fluids, the generalized rheological approach is used and plug zone sizes and shapes are determined automatically whatever the eccentric annular The intuitive user interface shown in Fig. 4a geometry. requires only an elementary understanding of engineering vocabulary and the simulator may be operated with minimal training. Annular geometry is defined by entering center coordinates and radii in the upper left menu. Clicking 'Show Annulus' provides an instantaneous display of the geometry assumed, plus a typical curvilinear grid, e.g., as illustrated in Fig. 4b, whose mesh density may be coarsened or refined at In addition, online editing utilities allow the baseline eccentric circles to be edited for washout, cuttings bed or fracture modification effects.

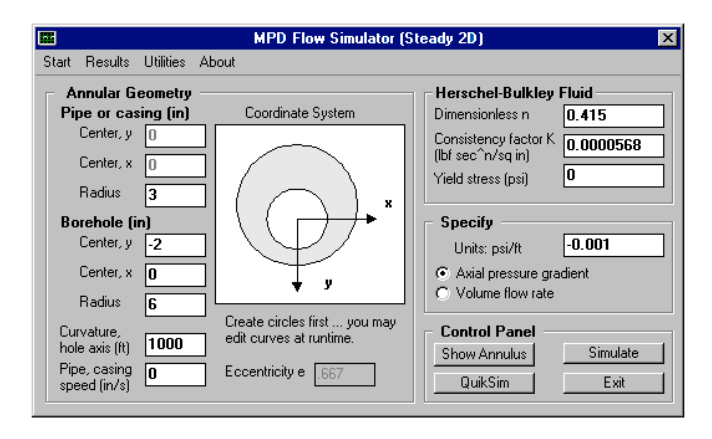


Fig. 4a - Steady flow user interface.

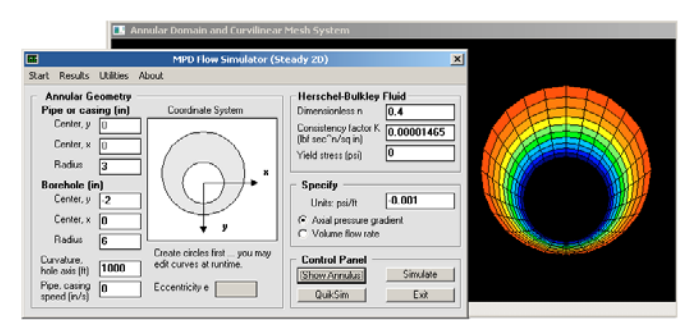


Fig. 4b - Quick annular geometry and curvilinear grid displays.

Rheological parameters for the general Herschel-Bulkley fluid are entered into the input boxes at the upper right of Fig. 4a. Four model are possible by choosing the values of n, K and τ_0 appropriately. Newtonian fluids require n=1 and $\tau_0=0$, while power law fluids allow general n with vanishing τ_0 . On the other hand, Bingham plastics require n=1 and non-vanishing τ_0 , while all three parameters may be generally assumed in the case of Herschel-Bulkley fluids. Fig. 4c also shows two utilities for n and K determination in the case of power law fluids, that is, assuming Fann dial readings or viscosity and shear rate data are available.

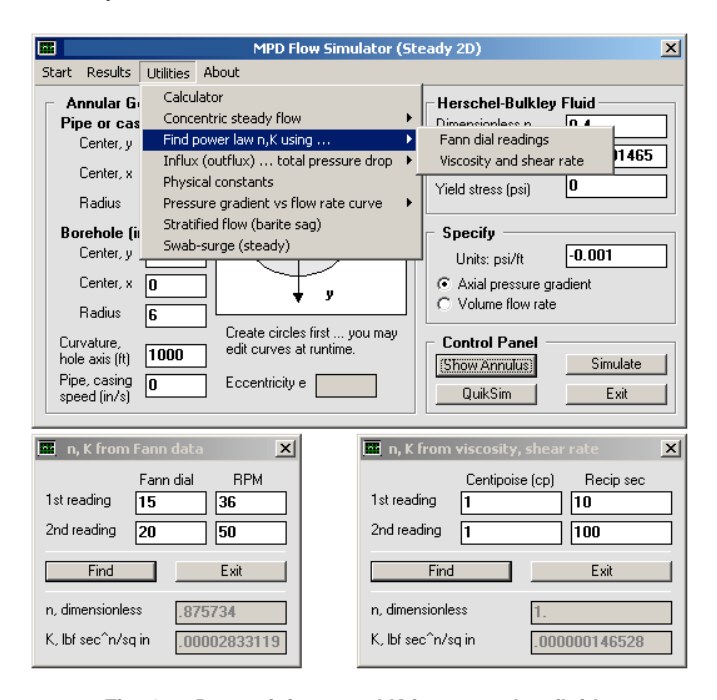


Fig. 4c – Determining n and K for power law fluids.

It is clear from Figs. 4a – 4c that several important auxiliary capabilities have been built into the overall algorithm. First, the axis of the borehole need not be straight; it may be curved, with any constant value for radius of curvature, to model short, medium and large radius turning of the borehole in offshore applications. This properly accounts for centrifugal effects which will affect the relationship between pressure gradient and volume flow rate.

Second, the drillpipe may move in either direction

relative to the borehole, that is, constant speed translational motion is permitted. In the simplest application, the drillstring penetrates the formation, moves relative to the borehole at constant positive or negative speed, and induces a purely two-dimensional flow everywhere; the value of this speed is entered into the bottom left input box of Fig. 4a. This capability also supports steady-state swab-surge analysis, with the mudpumps turned off or on and continuously running, as will be illustrated in examples later. A simple 'Worksheet' is loaded by clicking 'Swab-surge (steady)' in Fig. 4c, which prompts the user for tripping mode and speed. The positive or negative induced volume flow rate is calculated and added to the flow rate specified at the mud pump. Two calculation modes described in the next paragraph was developed for swab-surge and other drilling and cementing applications.

The option boxes immediately above the 'Control Panel' in Fig. 4a show how two computational modes are supported. In the first, the applied axial pressure gradient is specified and volume flow rate (together with detailed field solutions for all physical properties) is calculated. In the second, volume flow rate is specified and pressure gradient (together with all field properties again) is determined iteratively. The algorithm involves some subtlety because, as will be described in the application for swab-surge, the directions for drillpipe motion and net volume flow rate need not be correlated. For the "flow rate specified" mode, an initial pressure gradient is assumed for which a test rate is calculated and compared against the target rate; if the results do not satisfy a tolerance of 1%, a half-step correction procedure is applied to the test gradient and the calculations are repeated to convergence. Typically, the "pressure gradient specified" mode requires 2-3 seconds or less for a complete solution, while the "flow rate specified" mode may require up to ten seconds.

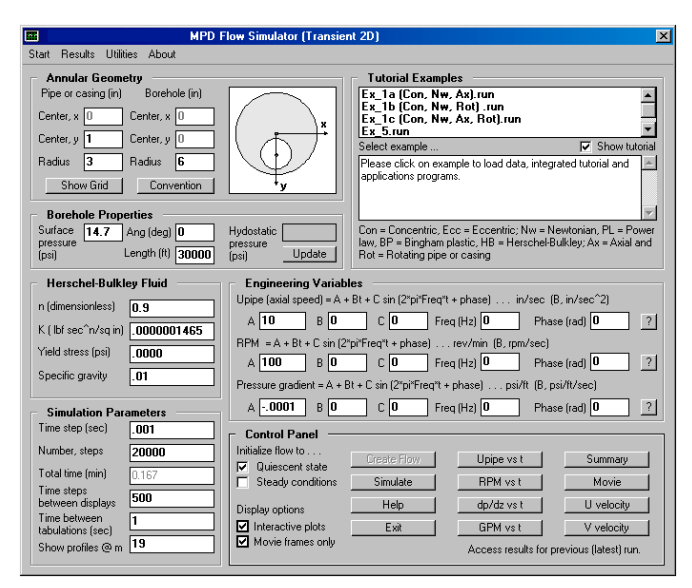


Fig. 4d - Transient flow user interface.

The foregoing remarks, focusing on the screen shot in Fig. 4a, apply to the steady flow simulator. The corresponding

user interface for transient incompressible flow is shown in Fig. 4d. Now, instead of Eq. 4, fully unsteady effects are computed from its transient extension, but rewritten in custom curvilinear coordinates applicable to the particular geometry under consideration. The above menu contains similar geometry and rheology definition modules, however, general, coupled, transient functions for pipe or casing axial reciprocation, inner circle rotation and pressure gradient are permitted. Additional input boxes for time step selection to facilitate numerical time integration are shown. Importantly, a database of prior runs is offered for user convenience and education. Clicking on a named entry at the top right of Fig. 4d automatically fills in all relevant input boxes and launches any sub-applications programs that are required. Users may edit numerical values and re-run any simulations available in the database. Also, all graphical capabilities described in this paper for steady flow are also available for unsteady flows.

Color displays of engineering properties. In order to make the mathematical models useful, every effort was expended to automate the display of important field quantities using two and three-dimensional color graphics. Use of the presentation tools is completely transparent to the engineer. An 'Install Graphics' button installs all required software quickly in a single pass; in addition, user training in operating the integrated graphical capabilities is not required. On convergence of the solution, a message box (supplemented with speech output and suggestions) summarizes basic pressure gradient and flow rate relationships.

The menu in Fig. 5a indicates that text output and color displays for different physical quantities are available for display. These quantities are post-processed from the velocity solution and made available for important engineering reasons. For example, Chin (1992, 2001) shows that apparent viscosity is vital to evaluating spotting fluid effectiveness in freeing stuck pipe. On the other hand, viscous stress (at the cuttings bed) is important to studying hole cleaning in horizontal and deviated wells, while velocity and viscosity play dominant roles in vertical well cuttings transport. A complete discussion, together with validations from a number of experimental investigations, is offered in Chin (1992, 2001).

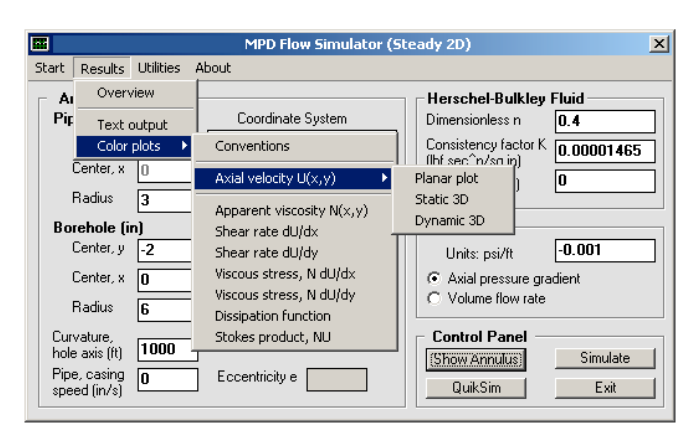


Fig. 5a - Graphical solution display options.

Fig. 5b displays results for axial velocity, apparent viscosity, shear rate, viscous stress, dissipation function and Stokes product in simple "planar plots." For the all-important velocity results, additional displays using three-dimensional color capabilities are offered as indicated in Fig. 5c. These capabilities, which include contour plots and mouse-rotatable perspective displays, are available for all mesh combinations, ranging from coarse to fine, selected by the user at run-time. These tools, plus text output, are useful in supporting detailed report generation.

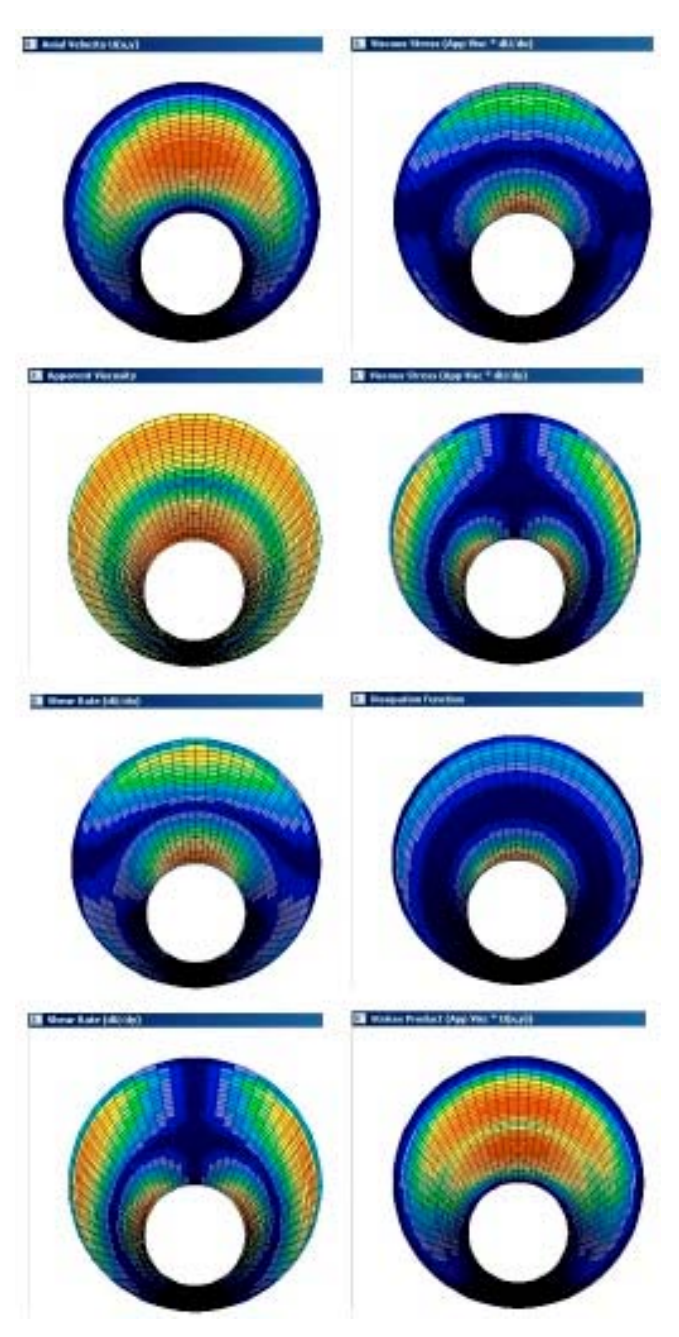


Fig. 5b - Planar color displays of key physical field quantities.

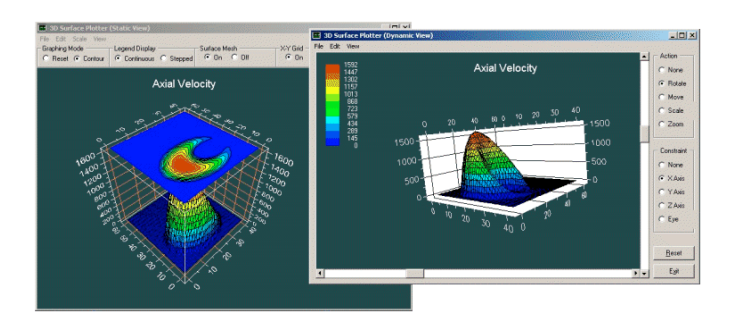


Fig. 5c – Three-dimensional, color displays (contour maps and mouse-rotatable perspective views).

Modeling borehole geometric irregularities. convenience, the main input screen in Fig. 4a accepts offcentered circles only. When center coordinates and radii are entered for inner and outer circles, an information box displays the calculated value for dimensionless eccentricity, to provide a useful reference point for drilling applications. Built-in error checking prevents circle cross-overs. At runtime, both inner and outer circle coordinates may be changed at the user's option. As shown in Fig. 6a below, existing contour coordinates are displayed, which may be modified without restriction. The changes elected for the example shown invoke changes to seven points only, in order to describe a simple washout; this convenient online editing tool can be used to draw washouts, cuttings beds and fracture indentations of any shape. While Fig. 6a provides a simple "planar plot" of velocity, Fig. 6b provides more detailed threedimensional resolution. Interestingly, for the simulation shown, the presence of the washout allows a 30% increase in flow rate for the same pressure gradient. General conclusions are not possible, and appropriate results must be made on a case-by-case basis.

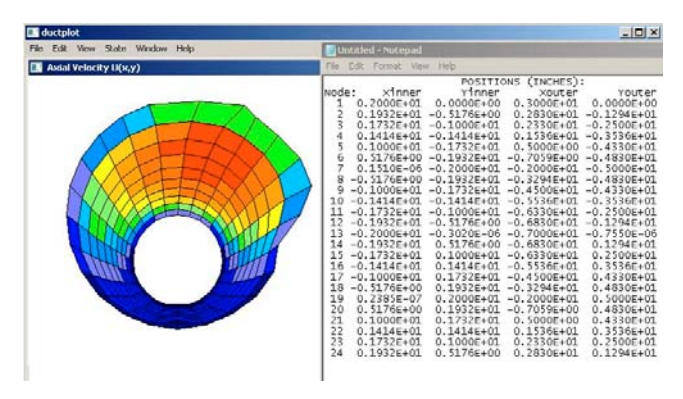


Fig. 6a - Modifying eccentric circle at run-time for washouts.

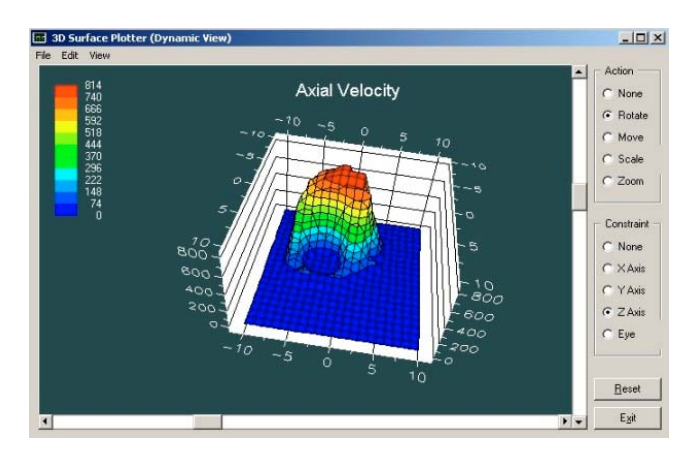


Fig. 6b - Color display of velocity field with washout.

Yield stress modeling. As noted earlier, yield stress modeling in eccentric annuli is important to both drilling and cementing applications. The use of the generalized Herschel-Bulkley constitutive model correctly predicts plug zone size and shape for all geometries. Because a continuous flow model is used, which guides the evolution of a single continuous velocity field, the computational difficulties associated with distinct internal boundaries and infinite viscosities are avoided. The method, we emphasize, will predict realistic plug zones with rapid gradients when they exist, as shown in Fig. 7a.

More interesting results are shown in Fig. 7b, in which plug zones for (1) a stationary pipe, (2) a pipe moving opposite to the direction of net flow, and (3) a pipe moving in the same direction of the main flow, are shown. Such computations are important in swab-surge applications and accurate pressure modeling. Plug zones associated with yield stress, of course, are important to understanding cuttings transport in drilling and fluid mixing in cementing. Again, no special procedures are required on the part of the user, as all dynamical features are computed automatically for both yield stress and non-yield fluids. Computation of plug zone flows requires no additional effort in terms of processing time and memory resources.

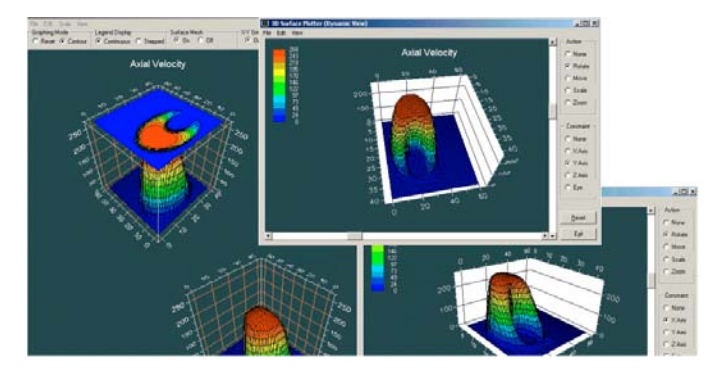


Fig. 7a – Typical velocity results for eccentric annulus with plug flow.

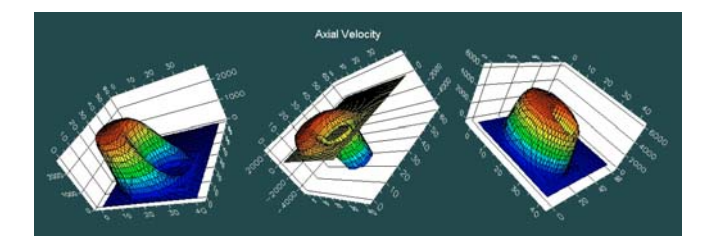


Fig. 7b – Non-Newtonian plug flow velocity profiles with stationary pipe (left), pipe moving opposite to flow (middle), and pipe moving with flow (right).

Rotating Flow Theory, Solution and Applications

Examples 2-1 and 2-2 provide scientific and mathematically oriented discussions (plus governing partial differential equations) that explain the apparent conflicts noted in the Abstract. Why does the early literature, that is, solutions developed largely by very eminent mathematicians and scientists, state that the effect of rotation (with pressure gradient fixed) is an increase in flow rate, a conclusion at the time supported by field observation? And why is the opposite quoted in almost all recent works?

In short, the early solutions and applications applied to concentric annular flow, for which the nonlinear convective terms in the axial momentum equation vanish identically. However, recent field observations apply to deviated and horizontal wells which host eccentric annular geometries, for which special terms that depend on rotation are always retained and never vanish. This was noted early on in the research, and again, the theoretical development is given in Examples 2-1 and 2-2.

These ideas can be developed further and provide the groundwork for steady and unsteady flows with and without rotation for general eccentric annuli and non-Newtonian rheologies. This is pursued in curvilinear coordinates to support the methodology used for the calculations. However, for the second part of the transient flow presentation, eight detailed computations are given, namely, Example 7-5 to Example 7-12.

The presentation provides all the details of the theoretical and numerical models, plus highly validated computed examples, and further, demonstrate that realistic flows such as those encountered in field operations can be computed stably, quickly, and with little user experience through the intuitive software interface developed.

More importantly are new capabilities for managed pressure drilling implications in well control. Conventionally, pressure at the drillbit (and, for that matter, along the entire length of the borehole) is controlled by adjusting mud rheology (by changing the mud), by controlling pumping speeds (to affect dynamic pressure loss), or by changing the pressure level at the surface choke, or all of the above. This work demonstrates that pipe rotation affects pressure drop (when rate is fixed) or rate (when pressure gradient is given) and we have explained why the calculations work. This implies that pipe rotation provides still another weapon in the arsenal to control well safety and formation integrity. Not all

wells can or should be controlled by adjusting rotation, of course, but the option now exists – and the means for using it as a practical tool that can be modeled by job planning software based on sound physical principles is available.

Part I: Theory

For readers who wish to proceed directly to the theoretical conclusions, explained in "plain English" without mathematics, please turn to the summary on Pages 15-16.

Example 2-1. Newtonian flow circular cylindrical coordinates.

In this first example, we study simple Newtonian flows for which the laminar viscosity μ is constant. In practice, viscosity does depend on pressure and temperature, but we restrict the discussion to simpler processes for which these dependencies do not arise - by "constant," we imply that viscosity is not affected by the size or shape of the vessel, or by the applied pressure gradient or the flow rate, and that its value can be measured unambiguously in a simple viscometer - properties not applicable to flows of non-Newtonian fluids. In particular, we will explore the properties of Newtonian flows written in circular cylindrical coordinates – and simple visual inspections of the equations do lead to interesting and important conclusions. The so-called Navier-Stokes equations that apply are derived in standard textbooks, e.g., Schlichting (1968). When "r," "0" and "z" are radial, azimuthal and axial coordinates, v_r , v_θ and v_z are Eulerian velocities in these directions, F_r , F_{θ} and F_z are body forces in the same directions, ρ is the constant fluid density, p is pressure and t is time, the following general partial differential equations can be derived.

Momentum equation in r: (2-1-1)

$$\begin{array}{l} \rho\{\partial v_r/\partial t + v_r\,\partial v_r/\partial r + v_\theta/r\,\partial v_r/\partial \theta - v_\theta^{\,\,2}/r + v_z\,\partial v_r/\partial z\} = F_r - \partial p/\partial r + \mu\{\partial^2 v_r/\partial r^2 + 1/r\,\partial v_r/\partial r - v_r/r^2 + 1/r^2\,\partial^2 v_r/\partial \theta^2 - 2/r^2\,\partial v_\theta/\partial \theta + \partial^2 v_r/\partial z^2\} \end{array}$$

Momentum equation in
$$\theta$$
: (2-1-2)

$$\begin{split} &\rho\{\partial v_{\theta}/\partial t + v_r\partial v_{\theta}/\partial r + v_{\theta}/r\ \partial v_{\theta}/\partial \theta + v_rv_{\theta}/r + v_z\partial v_{\theta}/\partial z\} = F_{\theta} - 1/r\ \partial p/\partial \theta + \mu\{\partial^2 v_{\theta}/\partial r^2 + 1/r\ \partial v_{\theta}/\partial r - v_{\theta}/r^2 + 1/r^2\ \partial^2 v_{\theta}/\partial \theta^2 + 2/r^2\ \partial v_r/\partial \theta + \partial^2 v_{\theta}/\partial z^2\} \end{split}$$

Momentum equation in
$$z$$
: (2-1-3)

$$\begin{split} &\rho\{\partial v_z/\partial t + v_r\,\partial v_z/\partial r + v_\theta/r\,\partial v_z/\partial \theta + v_z\,\partial v_z/\partial z\} = F_z - \partial p/\partial z \\ &+ \mu\{\partial^2 v_z/\partial r^2 + 1/r\,\partial v_z/\partial r + 1/r^2\,\partial^2 v_z/\partial \theta^2 + \partial^2 v_z/\partial z^2\} \end{split}$$

Mass continuity equation:

$$\partial v_r/\partial r + v_r/r + 1/r \partial v_\theta/\partial \theta + \partial v_z/\partial z = 0 \tag{2-1-4}$$

These define four equations for the four unknowns v_r , v_θ , v_z and p. General solutions to these nonlinearly coupled partial differential equations do not exist. We emphasize that, while the above formulation is written in circular cylindrical coordinates, it does apply to flows past non-circular geometries (in principle, the flow through a star-shaped duct,

for instance, can be solved, although in practice, the solution would be extremely awkward). Understanding this, we ask what general conclusions can be drawn for concentric versus eccentric annular flows. For the remainder of this section, we will ignore the effects of externally imposed body forces, e.g., gravity, electric charge, etc.

Concentric, steady, two-dimensional flows without influx. We first address the most commonly formulated problem, namely, concentric annular flows without azimuthal dependence, so that $\partial/\partial\theta=0$ (this does not require that $v_\theta=0$); flows without fluid influx or outflux, for which $v_r=0$; then, those for which the problem is steady, so that $\partial/\partial t=0$; and finally, we invoke the restriction to purely two-dimensional flows whose properties do not vary from one cross-section to the next, so that $\partial/\partial z=0$. When these conditions are satisfied, the foregoing momentum equations reduce to Equations 2-1-5, 2-1-6 and 2-1-7, while Equation 2-1-4 for mass conservation is identically satisfied.

Momentum equation in r:

$$\partial p/\partial r = \rho v_{\theta}^2/r \tag{2-1-5}$$

Momentum equation in θ :

$$\partial^2 \mathbf{v}_{\theta} / \partial \mathbf{r}^2 + 1 / \mathbf{r} \, \partial \mathbf{v}_{\theta} / \partial \mathbf{r} - \mathbf{v}_{\theta} / \mathbf{r}^2 = 0 \tag{2-1-6}$$

Momentum equation in z:

$$\partial^2 \mathbf{v}_z / \partial \mathbf{r}^2 + 1/\mathbf{r} \ \partial \mathbf{v}_z / \partial \mathbf{r} = (1/\mu) \ \partial \mathbf{p} / \partial \mathbf{z} \tag{2-1-7}$$

We will provide mathematical and software solutions to these later, but for now, we emphasize their general properties. The linear azimuthal velocity field v_{θ} is determined by solving Equation 2-1-6 subject to constant values at the radial boundaries. At the inner pipe or casing surface, the speed is determined by rotation speed and radius, while at the outer annular wall, the speed is zero. Notice that the solution for v_{θ} does not involve $\partial p/\partial z$. In other words, the azimuthal motion is simply one induced by "dragging" at the inner pipe surface.

Now consider the solution for axial velocity found by the solution of Equation 2-1-7 subject to constant speeds at the radial boundaries, e.g., a zero or non-zero translational speed at the inner surface and zero at the outer wall. The solution does not involve the rotational speed, and includes μ and the applied pressure gradient $\partial p/\partial z$ only to the extent that they appear in the lumped form $(1/\mu)\ \partial p/\partial z$. In conclusion, the azimuthal motion does not affect axial flow and axial motion does not influence azimuthal flow: the two are dynamically independent. Only when v_θ is available is Equation 2-1-5 used, and then, only in computing a radial pressure gradient that arises from centrifugal effects. It is remarkable that such general properties can be derived simply by visual inspection without any knowledge of partial differential equations.

Eccentric, steady, two-dimensional flow. Now let us repeat this analysis without the assumption calling for concentric flow, that is, we no longer assume that $\partial/\partial\theta = 0$. In doing so, we may deal with cross-sections that contain eccentric circles, but the eccentric annuli may well contain

asymmetric washouts at the outer contour and arbitrary cuttings beds at the bottom contour. We will assume that $\partial/\partial t = \partial/\partial z = 0$ but no longer require $v_r = 0$. Then, we have

$$\label{eq:continuous_equation} \begin{split} &\textit{Momentum equation in } r : \\ &\rho\{\ v_r\,\partial v_r/\partial r + v_\theta/r\ \partial v_r/\partial \theta - v_\theta^2/r\ \} = -\ \partial p/\partial r \\ &+ \mu\{\partial^2 v_r/\partial r^2 + 1/r\ \partial v_r/\partial r - v_r/r^2 + 1/r^2\ \partial^2 v_r/\partial \theta^2 - 2/r^2\ \partial v_\theta/\partial \theta\} \\ &\textit{Momentum equation in } \theta : \end{split}$$

$$\begin{split} &\rho\{v_r\,\partial v_\theta/\partial r+v_\theta/r\,\partial v_\theta/\partial \theta+v_rv_\theta/r\,\}=-1/r\,\partial p/\partial \theta\\ &+\mu\{\partial^2 v_\theta/\partial r^2+1/r\,\partial v_\theta/\partial r-v_\theta/r^2+1/r^2\,\partial^2 v_\theta/\partial \theta^2+2/r^2\,\partial v_r/\partial \theta\}\\ &\textit{Momentum equation in z:}\\ &\rho\{v_r\,\partial v_z/\partial r+v_\theta/r\,\partial v_z/\partial \theta\,\}=-\partial p/\partial z\\ &+\mu\{\partial^2 v_z/\partial r^2+1/r\,\partial v_z/\partial r+1/r^2\,\partial^2 v_z/\partial \theta^2\,\} \end{split} \tag{2-1-10}$$

Mass continuity equation:
$$\partial v_r/\partial r + v_r/r + 1/r \partial v_\theta/\partial \theta = 0$$
 (2-1-11)

These remain four partial differential equations in four unknowns whereas Equations 2-1-6 and 2-1-7 are coupled, linear, ordinary differential equations. Hence, the solutions are extremely difficult to obtain. Now, we have not yet specified an annular geometry, nor have we defined the r- θ coordinate system that applies to the problem. Nonetheless, we can assume in a dimensionless sense that $v_{\theta} >> v_{r}$ so that v_{r} can be ignored in a first approximation. The main focus is the resulting momentum equation in z, which now takes the form

$$\frac{\partial^2 \mathbf{v}_z}{\partial \mathbf{r}^2 + 1/\mathbf{r}} \frac{\partial \mathbf{v}_z}{\partial \mathbf{r} + 1/\mathbf{r}^2} \frac{\partial^2 \mathbf{v}_z}{\partial \mathbf{\theta}^2} \approx (2-1-12)$$

$$\approx (1/\mu) \frac{\partial \mathbf{p}}{\partial z} + (\mathbf{p}/\mu)(\mathbf{v}_{\theta}/\mathbf{r}) \frac{\partial \mathbf{v}_z}{\partial \theta}$$

This should be compared with the earlier result in Equation 2-1-7, that is, $\partial^2 v_z/\partial r^2 + 1/r\ \partial v_z/\partial r = (1/\mu)\ \partial p/\partial z$. The left-side now includes an additional term " $1/r^2\ \partial^2 v_z/\partial \theta^2$." In fact, the left-hand operator can be written in the more familiar form " $\partial^2 v_z/\partial x^2 + \partial^2 v_z/\partial y^2$ " using rectangular coordinates, from which we recognize the standard Laplace operator. However, it is the right-side that is extremely interesting. No longer is the effective pressure gradient simply given by the constant value $(1/\mu)\ \partial p/\partial z$. Instead, this term is modified by the correction $(\rho/\mu)(v_\theta/r)\ \partial v_z/\partial \theta$, which we emphasize is proportional to the fluid density and the inner pipe rotation rate and is inversely proportional to viscosity.

What are the physical consequence of this modification? In the concentric problem, the total volume flow rate could be determined by integrating the product of v_z (from Equation 2-1-7) and " $2\pi r$ dr" over the annular domain. The result is proportional to $(1/\mu)$ $\partial p/\partial z$, with the constant of proportionality depending only on geometry. The flow rate does not depend on rotation speed. When eccentricity is permitted, however, the effects of pipe rotation are coupled nonlinearly. In addition, the correction to $(1/\mu)$ $\partial p/\partial z$ now depends on the lumped parameter "mud weight \times rpm / viscosity" in a nontrivial manner. The correction importantly depends on the spatial coordinates r and θ as well as the yet-to-be-determined solution $v_z(r,\theta)$: it is spatially variable and

volume flow rate will no longer depend on $(1/\mu) \partial p/\partial z$ alone. Thus, the effective pressure gradient changes from what we have in the concentric case. The flow rate will generally be different, and computations show that, for the same μ , $\partial p/\partial z$ and rpm, the effect of eccentricity is a strong reduction in flow. Note that this conclusion is obtained for a Newtonian fluid having constant viscosity. When non-Newtonian effects are considered, the competing effects of shear-thinning will enter and these will be discussed separately in Example 2-2.

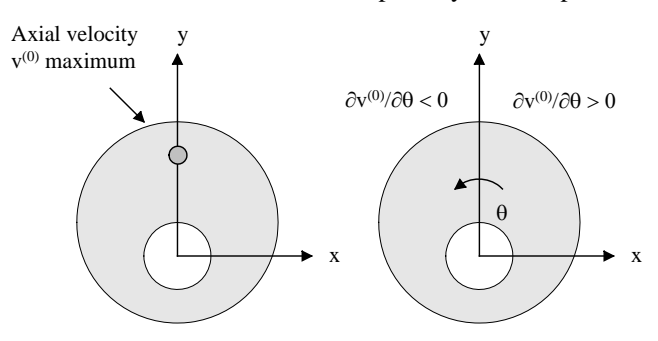


Figure 2-1-1. Location of axial velocity maximum in non-rotating flow.

Furthermore, because the correction also depends on $v_{\theta} \, \partial v_z \, / \partial \theta$, we expect that the location of the maximum in axial velocity (in an eccentric annulus with left-right symmetry) found at the wide side along the vertical line of symmetry, e.g., as shown at the left of Figure 2-1-1, will displace azimuthally, and it does, as a later explanation and all subsequent calculations will show.

It suffices to emphasize that eccentricity and rotation effects even for basic Newtonian fluids are extremely subtle. However, simple mathematical constructs can be devised to explore some of these subtleties and to facilitate fast numerical solutions. We explain an important one in the context of Equation 2-1-12 for v_z which we rewrite without the subscript "z" for clarity. In mixed coordinates, we have

$$\partial^2 v/\partial x^2 + \partial^2 v/\partial y^2 \approx (1/\mu) \partial p/\partial z + (\rho/\mu)(v_\theta/r) \partial v/\partial \theta$$
 (2-1-13)

Now, we separate "eccentric, non-rotating" from "eccentric, rotating" effects by isolating the inertia-dependent $(\rho/\mu)(v_\theta/r)~\partial v~/\partial \theta.$ In the language of mathematics, we introduce a "regular perturbation expansion" such that $v=v^{(0)}+v^{(1)}+\ldots$ in which the zeroth solution represents leading order concentric non-rotating effects and the first perturbation to it includes all others. Mathematical books that introduce this subject include the well known research monographs by Van Dyke (1964), Cole (1968) and Nayfeh (1973). If we next assume that

$$\partial^2 \mathbf{v}^{(0)} / \partial \mathbf{x}^2 + \partial^2 \mathbf{v}^{(0)} / \partial \mathbf{y}^2 = (1/\mu) \partial \mathbf{p} / \partial \mathbf{z}$$
 (2-1-14)

then subtraction of Equation 2-1-14 from Equation 2-1-13 with the series substitution leads to

$$\partial^2 v^{(1)} / \partial x^2 + \partial^2 v^{(1)} / \partial y^2 \approx (\rho/\mu)(v_\theta/r) \partial v^{(0)} / \partial \theta$$
 (2-1-15)

Now, the concentric solution to Equation 2-1-14, or Equation 2-1-7, is just the classical Poiseuille pipe flow

formula available in the general literature, e.g., Schlichting (1968). However, Equation 2-1-14 applies to eccentric problems too, and its exact numerical solution for arbitrary geometries the subject of this paper and one of the simulators.

But we do not need to solve it to understand its implications. We have shown an eccentric annulus at the left of Figure 2-1-1 with left-right symmetry. We can imagine that we now have obtained a straight, non-rotating, "out of the page" axial flow solution v⁽⁰⁾ applicable to the left diagram. The location of maximum axial speed is shown at the gray dot. With the θ convention highlighted, it is clear that $\partial v^{(0)} / \partial \theta$ increases at the right of the line of symmetry while it decreases at the left. Next, observe that the sign of the azimuthal velocity v_{θ} in Equation 2-1-15 cannot change. Thus, $(\rho/\mu)(v_{\theta}/r) \partial v^{(0)}/\partial \theta$, which functions as an effective pressure gradient for the disturbance axial flow v(1), is antisymmetric with respect to the vertical line of symmetry: it subtracts flow on one side and adds at the other. This effective pressure gradient is variable throughout the annular cross-section. This driver, which depends on the solution to the azimuthal problem, affects total flow rate in a nontrivial way, although for small values of "mud weight x rpm / viscosity," it is clear that the solution is proportional to it with the v⁽¹⁾ field again being antisymmetric. This antisymmetry means that "mud weight x rpm / viscosity" does not significantly affect total flow rate if it is small. However, when it is large, the symmetry and antisymmetry ideas may break down. It is also clear how, in the presence of unsteady effects, arguments like those offered above are not possible.

We note that, while we have provided useful discussions on rotation and eccentricity, the numerical solution for steady rotating flows in eccentric domains, even under the assumption of simplified Newtonian flow, has proven to be challenging. A limited number of papers on the subject have been published by several authors, but these have offered few formulation and numerical details, and have declined to discuss computing times and numerical stability properties. The author, in fact, has written a steady, rotating flow solver for non-Newtonian eccentric annular flows, which converges for vz under restrictive conditions. The controlling "mud weight × rpm / viscosity" parameter, for the larger values characteristic of those parameters used in practical drilling and cementing, always leads to numerical instability. On the other hand, the perturbation problem for v_z⁽¹⁾ could be solved with unconditional stability; however, the linearization used clearly does not apply physically to high values of "mud weight x rpm / viscosity." In this paper, however, steady-state flows with rotation are successfully solved by integrating the transient equations asymptotically in time until steady conditions are reached using a fast solver.

Example 2-2. Shear-thinning and non-Newtonian flow effects.

In the previous example, we studied Newtonian flows for which viscosity always remained constant to focus on the effects of rotation and eccentricity alone. Here we consider non-Newtonian fluids which generally exhibit shear-thinning, but do not discuss rotation, so that we remove the convective effects of inertia. Whereas before, the use of circular cylindrical coordinates facilitated an understanding of pipe rotation, we now introduce rectangular or Cartesian coordinates to assist in explanations of non-Newtonian viscosity effects. We consider here eccentric annular flows formed by general closed curves (which need not be circular), but for simplicity, restrict the discussion to steady, two-dimensional, single-phase flows. These assumptions are removed later.

The equations for general fluid motions in three dimensions are available from many excellent textbooks (Bird, Stewart and Lightfoot, 1960; Streeter, 1961; Schlichting, 1968; and, Slattery, 1981). We cite these without proof. For problems without inner pipe rotation, it turns out that their rectangular form is most suitable in deriving curvilinear coordinate transforms – as we later show, the relevant starting point for rotation effects is cylindrical radial coordinates.

Governing equations. Let u, v and w denote Eulerian fluid velocities, and F_z , F_y and F_x denote body forces, in the z, y and x directions, respectively, where (z,y,x) are Cartesian coordinates. Also, let ρ be the constant fluid density and p be the pressure; we denote by S_{zz} , S_{yy} , S_{xx} , S_{zy} , S_{yz} , S_{xz} , S_{zx} , S_{yx} and S_{xy} the nine elements of the general extra stress tensor $\underline{\mathbf{S}}$. If t is time and ∂ 's represent partial derivatives, the complete equations of motion obtained from Newton's law and mass conservation are,

Momentum equation in z:

$$\begin{array}{ll} \rho \left(\partial u / \partial t + u \; \partial u / \partial z + v \; \partial u / \partial y + w \; \partial u / \partial x \right) \; = \\ = F_{Z} - \partial p / \partial z + \partial S_{ZZ} / \partial z + \partial S_{ZY} / \partial y + \partial S_{ZX} / \partial x \end{array} \tag{2-2-1}$$

Momentum equation in y:

$$\begin{split} \rho \left(\partial v / \partial t + u \ \partial v / \partial z + v \ \partial v / \partial y + w \ \partial v / \partial x \right) &= \\ &= F_{\mathbf{V}} - \partial p / \partial y + \partial S_{\mathbf{VZ}} / \partial z + \partial S_{\mathbf{VV}} / \partial y + \partial S_{\mathbf{VX}} / \partial x \end{split} \tag{2-2-2}$$

Momentum equation in x:

$$\begin{split} &\rho\left(\partial w/\partial t + u \; \partial w/\partial z + v \; \partial w/\partial y + w \; \partial w/\partial x\right) = \\ &= F_{\mathbf{X}} - \partial p/\partial x + \partial S_{\mathbf{X}\mathbf{Z}}/\partial z + \partial S_{\mathbf{X}\mathbf{V}}/\partial y + \partial S_{\mathbf{X}\mathbf{X}}/\partial x \end{split} \tag{2-2-3}$$

Mass continuity equation:

$$\partial \mathbf{u}/\partial \mathbf{z} + \partial \mathbf{v}/\partial \mathbf{y} + \partial \mathbf{w}/\partial \mathbf{x} = 0 \tag{2-2-4}$$

Simple rheological models. These equations apply to all Newtonian and non-Newtonian fluids. In continuum mechanics, the most common class of empirical models for incompressible, isotropic fluids assumes that $\underline{\mathbf{S}}$ can be related to the rate of deformation tensor $\underline{\mathbf{D}}$ by a relationship of the form

$$\mathbf{S} = 2 \,\mathrm{N}(\Gamma) \,\mathbf{D} \tag{2-2-5}$$

where the elements of \mathbf{D} are

$$D_{zz} = \partial u/\partial z \qquad (2-2-6)$$

$$D_{yy} = \partial v/\partial y \qquad (2-2-7)$$

$$D_{xx} = \partial w/\partial x \qquad (2-2-8)$$

$$D_{xy} = D_{xy} - (\partial x/\partial x + \partial y/\partial x)/2 \qquad (2-2-8)$$

$$D_{\mathbf{Z}\mathbf{y}} = D_{\mathbf{y}\mathbf{z}} = (\partial \mathbf{u}/\partial \mathbf{y} + \partial \mathbf{v}/\partial \mathbf{z})/2$$

$$D_{\mathbf{Z}\mathbf{y}} = D_{\mathbf{y}\mathbf{z}} = (\partial \mathbf{u}/\partial \mathbf{x} + \partial \mathbf{w}/\partial \mathbf{z})/2$$
(2-2-10)

$$\begin{array}{ll} D_{xx} & D_{yz} = D_{yz} = (\partial u/\partial y + \partial v/\partial z)/2 & (2-2-9) \\ D_{zx} & D_{xz} = (\partial u/\partial x + \partial w/\partial z)/2 & (2-2-10) \\ D_{yx} & D_{xy} = (\partial v/\partial x + \partial w/\partial y)/2 & (2-2-11) \end{array}$$

In Equation 2-2-5, $N(\Gamma)$ is the "apparent viscosity" satisfying $N(\Gamma) > 0$

 $\Gamma(z,y,x)$ being a scalar functional of u, v and w defined by the tensor operation

$$\Gamma = \{ 2 \operatorname{trace} \left(\underline{\mathbf{D}} \bullet \underline{\mathbf{D}} \right) \}^{1/2}$$
 (2-2-13)

Unlike the constant laminar viscosity u in classical Newtonian flow, we will demonstrate that the apparent viscosity depends on the details of the particular problem being considered, e.g., the rheological model used, the exact annular geometry occupied by the fluid, the applied pressure gradient or the net volume flow rate. Also, it varies with the position (z,y,x) in the annular domain. measurements obtained from viscometers are usually not meaningful in practice. In fact, inferences can be very misleading.

Examples. To fix ideas, consider the simple but important Ostwald-de Waele model for two-parameter "power law" fluids, for which

$$N(\Gamma) = K \Gamma^{n-1} \tag{2-2-14a}$$

where the "consistency factor" K and the "fluid exponent" n are constants. Such power law fluids are "pseudoplastic" when 0 < n < 1. Newtonian when n = 1, and "dilatant" when n > 1. Most drilling fluids are pseudoplastic. In the limit (n = 1, $K=\mu$), Equation 2-2-14a reduces to the Newtonian model with $N(\Gamma) = \mu$, where μ is the constant laminar viscosity; in this classical limit, stress is directly proportional to the rate of strain. Only for Newtonian flows is volume flow rate a linear function of applied pressure gradient and inversely proportional to μ .

Power law and Newtonian fluids respond instantaneously to applied pressure and stress. But if the fluid behaves as a rigid solid until the net applied stresses have exceeded some known critical yield value, say S_{vield}, then Equation 2-2-14a can be generalized by writing

$$\begin{split} & N(\Gamma) = K \; \Gamma^{n-1} + S_{yield} / \Gamma \; \text{if} \; \{1/2 \; \text{trace} \; (\underline{\underline{S}} \bullet \underline{\underline{S}})\}^{1/2} > S_{yield} \\ & \underline{\underline{D}} = 0 \; \text{if} \; \{1/2 \; \text{trace} \; (\underline{\underline{S}} \bullet \underline{\underline{S}})\}^{1/2} < S_{yield} \end{split} \tag{2-2-14b}$$

In this form, Equation 2-2-14b rigorously describes the Herschel-Bulkley fluid. When the limit $(n=1, K=\mu)$ is taken, the first equation becomes

$$N(\Gamma) = \mu + S_{yield}/\Gamma \text{ if } \{1/2 \text{ trace } (\underline{\underline{\mathbf{S}}} \bullet \underline{\underline{\mathbf{S}}})\}^{1/2} > S_{yield} \qquad (2\text{-}2\text{-}14c)$$

This is the Bingham plastic model, where μ is now the "plastic viscosity." For Herschel-Bulkley and Bingham plastic flows in circular pipes, exact analytical solutions can be developed for velocity distribution, plug zone radius, and total flow rate

(these limits include Newtonian and power law fluids). Analogous solutions are available for flows between parallel plates. Exact solutions for concentric annuli are available in closed analytical form and used to validate numerical flow models.

For illustrative purposes, we examine a limit of twodimensional power law flows, where the axial velocity u(y,x) does not depend on the axial coordinate z. In the absence of rotation, the velocities v and w in the cross-plane satisfy v = w= 0, so that the functional Γ in Equation 2-2-14a takes the

$$\Gamma = [(\partial u/\partial y)^2 + (\partial u/\partial x)^2]^{1/2}$$
(2-2-15)

and Equation 2-2-14a becomes

$$N(\Gamma) = K \left[(\partial u/\partial y)^2 + (\partial u/\partial x)^2 \right]^{(n-1)/2}$$
 (2-2-16)

The apparent viscosity reduces to the conventional $N(\Gamma) = K$ $(\partial u/\partial y)^{(n-1)}$ formula for one-dimensional, parallel plate and "slot flow" flows considered in the literature. When both independent variables y and x for the cross-section are present, as in the case for eccentric annular flow, significant mathematical difficulty arises. For one, the ordinary differential equation for annular velocity in simple concentric geometries becomes a partial differential equation. And whereas the former requires boundary conditions at two points, the partial differential equation requires no-slip boundary conditions imposed along two arbitrarily closed curves. The nonlinearity of the governing equation and the irregular annular geometry only compound these difficulties. Despite these, the resulting problem is simple in a sense. The momentum equations for v and w vanish identically and that for mass conservation implies that u = u(y,x) only. The single remaining equation is

$$\partial S_{ZV}/\partial y + \partial S_{ZX}/\partial x = \partial P/\partial z = constant$$
 (2-2-17)

where the constant pressure gradient $\partial P/\partial z$ is prescribed. This is to be compared to the simpler Equation 2-1-7. Since $\mathbf{S} =$ 2N**D**, this reduces to

$$\partial (N \partial u/\partial y)/\partial y + \partial (N \partial u/\partial x)/\partial x = \partial P/\partial z$$
 (2-2-18)

Substitution of Equation 2-2-16 shows that Equation 2-2-18 can be written as a nonlinear Poisson equation, that is, as Equation 2-1-19, in the form

$$\begin{array}{l} \partial^2 u/\partial y^2 + \partial^2 u/\partial x^2 = [\partial P/\partial z + (1\text{-}n)N(\Gamma)(u_y{}^2u_{yy} \\ + 2u_yu_xu_{yx} + u_x{}^2u_{xx})/(u_y{}^2 + u_x{}^2)] \ / \ N(\Gamma) \end{array} \eqno(2\text{-}2\text{-}19)$$

which is to be compared with Equation 2-1-14. This equation, together with extensions for rotation and complicated rheological effects, is solved exactly in the software models. The only purpose in writing down explicitly here is to provide a "live" example showing why nonlinear effects are complicated.

The Newtonian limit with n = 1 reduces Equation 2-2-19 to the classical Poisson equation $\partial^2 \mathbf{u}/\partial \mathbf{v}^2 + \partial^2 \mathbf{u}/\partial \mathbf{x}^2 = (1/\mu)$ $\partial P/\partial z$ with several important properties. For example, doubling pressure gradient while doubling the viscosity leaves u(y,x) unchanged: only the lumped driver $(1/\mu) \partial P/\partial z$ appears. And, for instance, doubling $\partial P/\partial z$ with μ constant will double u everywhere, a property obvious from simple rescaling. Also, μ is just the quantity measured in a viscometer, and its value remains unchanged for all pressure gradients and flow cross-sections.

However, when n is not unity, the "mess" at the right of Equation 2-2-19 remains. Casual observation leads us to conclude, for example, that doubling the pressure gradient will do something unclear, but what, is uncertain. Because the divisor of $\partial P/\partial z$ is not just a constant " μ ," but a complicated function which, because it depends on the as-yet unknown solution u(y,x), the so-called "apparent viscosity" is unknown. In fact, it will vary from problem to problem, and it will depend on the applied pressure gradient, plus the size and shape of the vessel, and it will be variable throughout the flow cross-section. Hence, we have the origin of the terms "shearthickening" and "shear-thinning." Shear-thickening and shear-thinning fluids are non-Newtonian, as their viscosities increase or decrease, respectively, as the applied shearing "Silly Putty" is shear-thickening, while stress increases. ketchup is shear-thinning.

It is important to note, from Equation 2-2-17, that fluid density ρ completely disappears in this steady flow without rotation. However, it is important that, from Example 2-1, density remains important when the flow rotates because the nonlinear convective terms do not vanish. It also goes without saying that density effects are all-important in transient analysis because inertia is important. We will demonstrate later that steady flows can be computed from unsteady algorithms using small densities for rapid convergence – but, this strategy is applicable only when there is no underlying pipe rotation.

Only n and K (and not "\mu") are "absolutes" for power law flow modeling which can be obtained from viscometer measurements. The foregoing difficulties apply not just to power law fluids, but to all non-Newtonian fluids, with or without yield stress. When yield stresses are present, other complications arise, e.g., the inability to identify *a priori* the size and shape of the plug zone means that such problems cannot be solved for practical annular geometries. We do, fortunately, offer a rigorous solution to this problem later.

In summary, we offer several general principles from the discussions of Examples 2-1 and 2-2. In particular,

- In Newtonian flow, the viscosity is a constant of the motion (barring changes due to pressure and temperature) which is unambiguously determined from viscometer measurement.
- In non-rotating Newtonian flow, the lumped quantity
 (1/μ) ∂p/∂z controls the dynamics, and changes to it will
 proportionally change u(y,z) everywhere thus, faster
 testing with inexpensive fluids, together with simple
 arithmetic extrapolation, can be used in engineering
 design.

- For concentric annuli in steady Newtonian rotating flow, azimuthal velocities do not depend on pressure gradient, and axial flows are unaffected by rotation: the two are dynamically uncoupled.
- Annular eccentricity introduces changes to the applied pressure gradient that are variable throughout the flow domain (the velocity likewise scales differently at different cross-sectional locations) when rotation is allowed. Their magnitudes are proportional to the product "density × rpm / viscosity." This effect generally decreases the flow rate (as rotation speed increases) for a fixed pressure gradient this nontrivial modification applies even to simple Newtonian fluids without shearthinning.
- Non-Newtonian fluids (even without rotation and three-dimensionality) exhibit shear-thickening and shear-thinning properties. In a concentric annulus with a rotating inner pipe, drilling fluid viscosity will decrease due to azimuthal motion so that net flow rate increases relative to the non-rotating case assuming that pressure gradient is fixed. Complications arise when this is countered by the effects of eccentricity computational methods are required to determine the exact balances between the two.
- Non-Newtonian flows in eccentric borehole annuli with rotation will exhibit shear-dependent changes to viscosity, plus changes to applied pressure gradient that depend on rotation speed, fluid density and viscosity (the "apparent viscosity" now varies throughout the flow domain). Simple rescaling arguments cannot be used to deduce flow properties for u(y,z) because the governing equations are extremely complicated in form.
- For non-Newtonian flows, laboratory testing and extrapolation is not possible because of the foregoing complications hence, the only recourse for prediction and job planning is full-scale testing with actual nonlinear fluids or, alternatively, detailed computational fluid-dynamics analysis.

Field and laboratory examples. Figures 2-2-1 and 2-2-2, together with the related discussions, are obtained from correspondence with John Lofton, Chevron, to whom the authors are grateful. Figure 2-2-1 provides a "pressure-while-drilling" (or, PWD) log from a field run. PWD logs provide real-time pressures as are conveyed to the surface with Measurement-While-Drilling tools and are essential to drilling safety. Such logs can monitor downhole conditions accurately and supply updates to calibrate software models used for planning.

Lofton writes, "Look at 1600 hrs on 25 April 02. After the connection at 1693' (red arrow), the pump is on (green curve) and the rotary is abruptly increased up to 100 RPM (red curve). The stand pipe pressure (blue curve) spikes – increased pump pressure. The ECD (red and black curves on

the far right) both increase. The rotation has increased the pump pressure and the annular friction for the same pump rate. This response seems consistent throughout the PWD log. This is a directional well from a platform with an angle of less than 45 degrees and is using a low density water based mud."

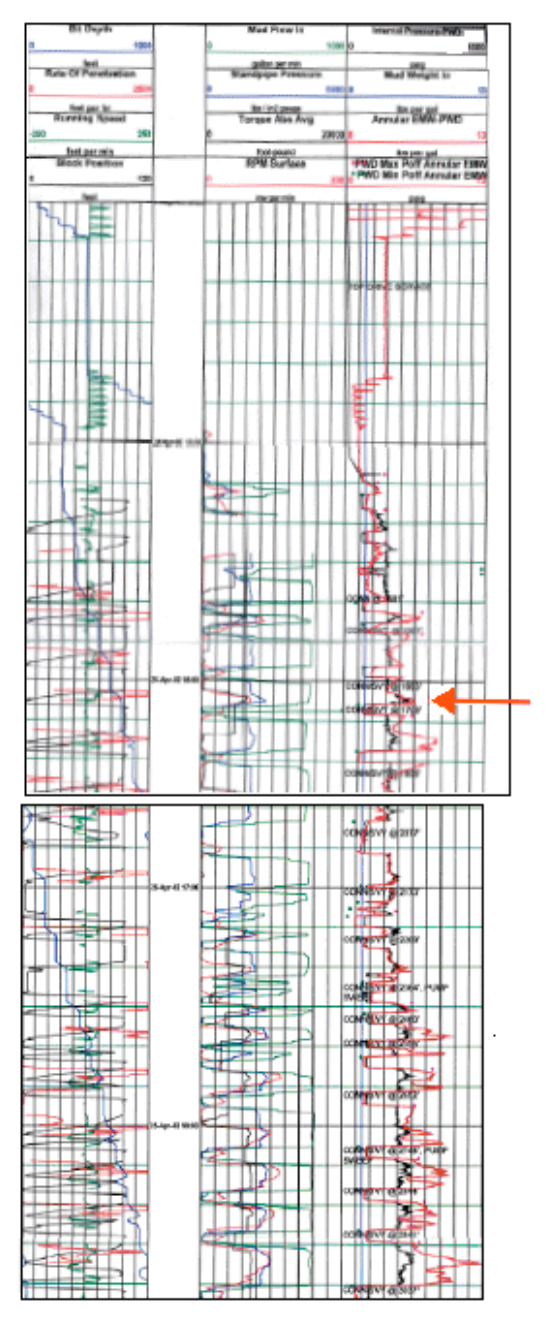


Figure 2-2-1. A "pressure-while-drilling" (PWD) log.

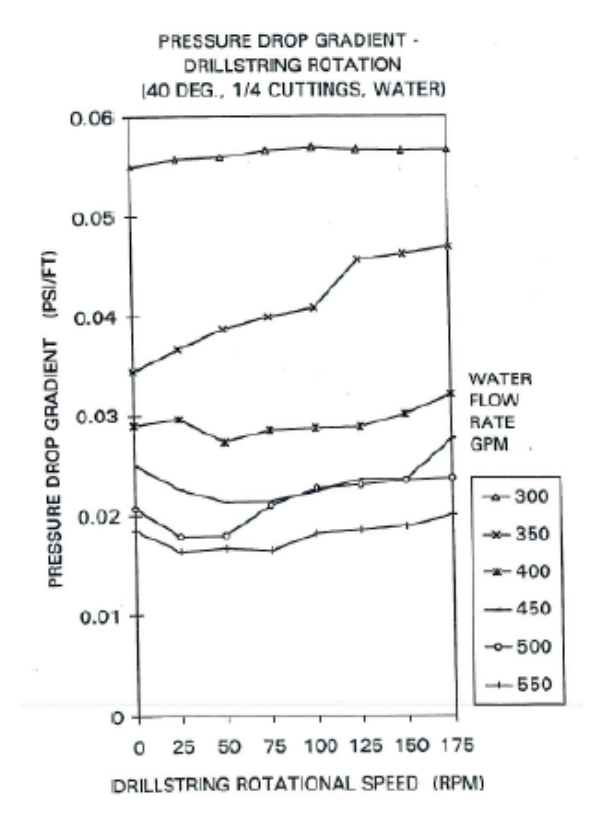


Figure 2-2-2. A laboratory example for 40° well.

"I have also looked at broader industry applications some of which I do not have first-hand, on-location experience. There was a study done at the University of Tulsa on the effects of rotation in inclined wellbores. I think it is excellent, honest work. No products to sell, no bias on the outcome. The effects of rotation were investigated at 40, 65, and 90 degrees of inclination. The annular pressure was monitored with rotation at each of these inclinations. The results at 40 degrees were similar to the PWD log above and reflects my experience in the field. Especially at the lower end of the flow-rates – 300 gpm and 350 gpm." (Results for 65° and 90° were more erratic, with some resulting in reduced pressure gradients – possibly because hole geometry changes due to unflushed cuttings.) The last comment on pronounced rotation effects at lower volume flow rates is especially significant. Lower flow rates point to high values of the dimensionless azimuthal-to-axial velocity ratio, a good indicator of rotation coupling to the overall flow. Many drillers have also indicated cuttings transport problems in larger diameter holes – large diameters are precisely the ones with smaller annular velocities. These two observations support the use of rotating pipe models in planning drilling jobs.

Part II: Calculated Examples

Example 7-5. Effect of steady-state rotation for Newtonian fluid flow in eccentric annuli.

Here we consider the effects of annular eccentricity. To isolate rheological effects, we assume a Newtonian fluid with constant viscosity so shear-thinning is impossible. The eccentricity is 0.333. As a validation point, we first obtain the flow rate under non-rotating conditions using the steady-state, curvilinear grid flow solver in Figure 7-5a. For the assumptions shown, the flow rate is 109.2 gpm (the parameters corresponding to the "engineering variables" not shown are identically zero). Next, we run the transient simulator for the same non-rotating flow conditions, as shown in Figure 7-5b, to obtain a nearly identical flow rate of 107.2 (the difference is less than 2%). The agreement is excellent.

Now, we importantly ask, "What if the drillpipe or casing were rotated? Does the flow rate increase or decrease, assuming the same pressure gradient?" In Figure 7-5c, we assume a somewhat high 400 rpm to demonstrate numerical stability, but also the fact that the asymptotic steady flow rate decreases to 99.4 gpm, a flow rate reduction of about 8%. Thus, in the complementary problem where flow rate is specified and pressure gradient is to be determined, we can expect to see similar order-of-magnitude increases to pressure drop. These changes are significant to drilling safety in managed pressure drilling.

The exact decrease or increase depends on rheological and geometric parameters, and will vary from run to run. Differences as high as 50% have been observed. But why did flow rate increase in an example for concentric flow but decrease here? The explanation is simple. In the earlier example, the gpm increase was due to a decrease in non-Newtonian apparent viscosity arising from rotation; also, for concentric annuli, the inertia terms in the axial momentum equations vanish identically. In this example, the viscosity is constant and does not change. A non-vanishing " $\rho v/r \partial U/\partial \theta$ " inertia term is new. The azimuthal velocity v is proportional to rpm, while $\partial U/\partial \theta$ " is related to eccentricity. The term acts as a spatially variable pressure gradient modifier. These reasons are subtle but clear when we examine the governing partial differential equations. We chose Newtonian fluids in this example to isolate rheological effects in order to ascertain the importance of the rotating flow inertia terms alone.

In the Control Panel of Figure 7-5b, we checked "Initialize flow to quiescent state." This assumes vanishing initial flow. We now check "steady conditions" for the starting point. The simulator first calculates a steady non-rotating flow, and then at t=0, uses this flow to initialize time integrations. This corresponds to a non-rotating pipe that is suddenly rotated. Figure 7-5d shows how the flow rate decreases suddenly from 107.2 gpm to 99.4 gpm, highlighting the effects of rotation (computing time is about one second). Importantly, even for this high rotation rate, the transient algorithm for coupled axial and azimuthal movement is fast

and stable. The results also demonstrate the usefulness of numerical simulation in drilling safety and operations.

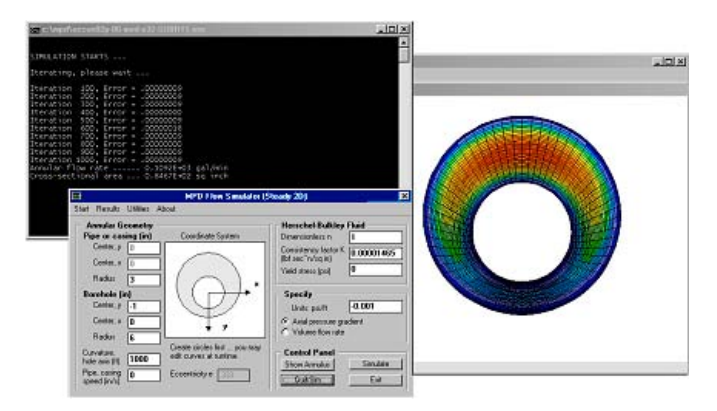


Figure 7-5a. Steady-state solution without rotation.

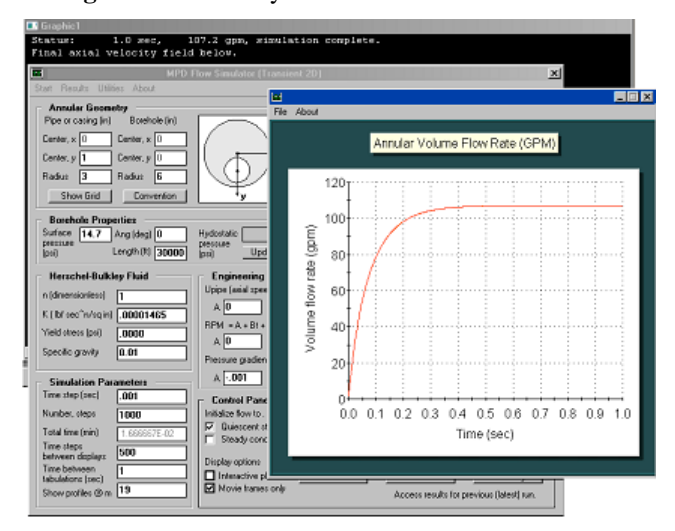


Figure 7-5b. Transient Newtonian solution without rotation.

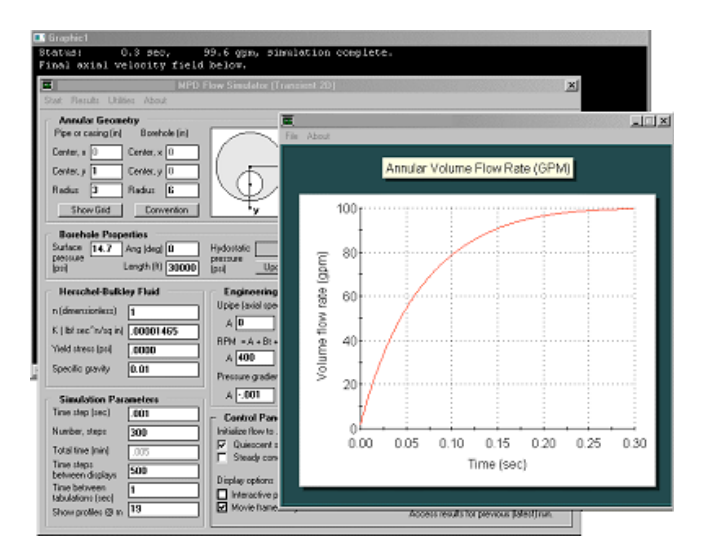


Figure 7-5c. Transient rotating solution from quiescent state (the curve actually peaks at 100 and asymptotes to 99.4 gpm).

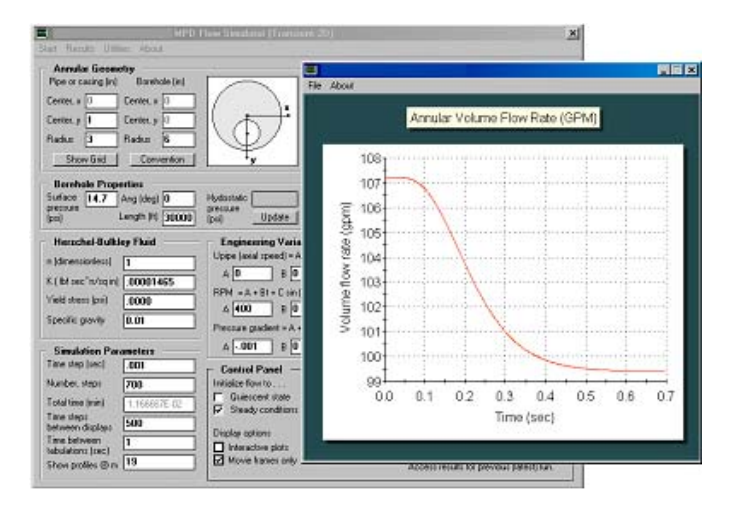


Figure 7-5d. Transient rotating solution from flowing state.

Example 7-6. Effect of steady rotation for power law flows in highly eccentric annuli at low densities (foams).

The annulus in Figure 7-5a, while not concentric, is not highly eccentric. In this example, we examine a cross-section with high eccentricity and also allow for nonlinear power law fluid motion. Here, the eccentricity is 0.5. Results for a nonrotating pipe are given in Figure 7-6a, where a steady flow rate of 1,052 gpm is indicated. The time required to achieve steady-state is approximately one second. What happens if we rotate the drillpipe at 300 rpm? Figure 7-6b shows that with rotation, the time to reach steady conditions is reduced; also, the flow rate decreases to 905.8 gpm. This suggests that in the complementary problem when volume flow rate is fixed, the effect of rotation is to increase (the absolute value of) pressure gradient. Consistent with the previous example, the decrease in flow rate occurs because of inertia effects. We emphasize that the flow rate reduction due to rotation seen here is a sizeable 16%. Finally, in Figure 7-6c, we re-run the simulation with the initial fluid assumed to be non-rotating and flowing. The results show an equilibration time of one second between steady states so that flow changes are sudden and dangerous. The steady-state flow rate is again about 900 gpm. There is a "bump" in the gpm vs time curve, one seen repeatedly in many such simulations. Whether or not this effect is real will require laboratory observation. All of the calculations for this example were performed stably, as the line graphs show, and required only 2-3 seconds of computing time.

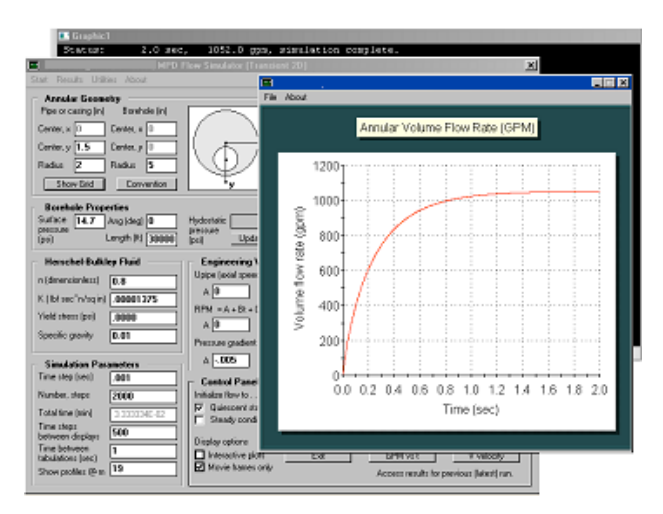


Figure 7-6a. Power law flow with non-rotating pipe.

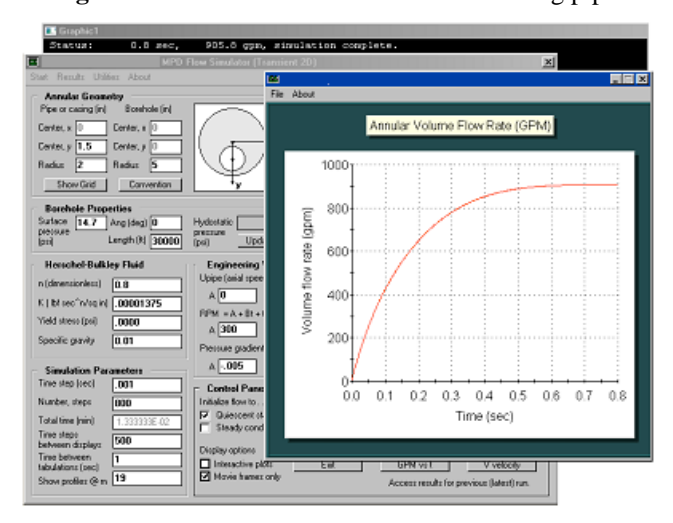


Figure 7-6b. Power law flow with rotating pipe (zero starting conditions).

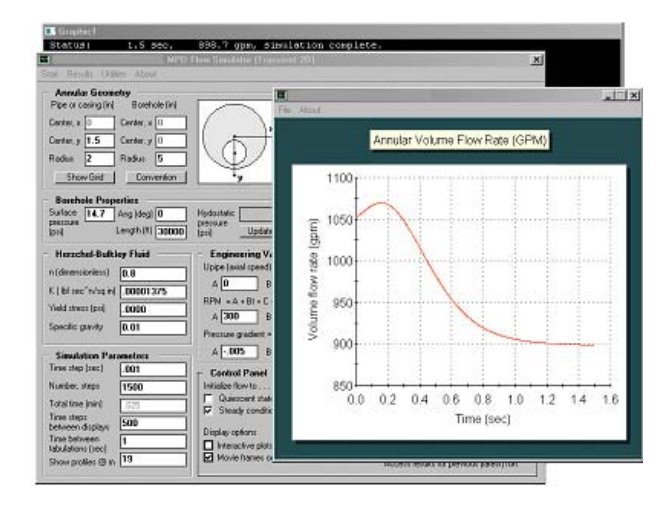


Figure 7-6c. Power law flow with rotating pipe (from flowing conditions).

It is important to point out some important software details associated with flow initialization. For steady flow formulations, the initial state of the flow does not appear as a parameter because there is no variation in time (actually, it does in a numerically sense, since initial solution guesses are taken, although internally to the software). For transient formulations, the initial state must be specified. If quiescent stagnant-flow conditions are selected, the box shown in Figure 7-6d is checked and "Simulate" can be clicked immediately.

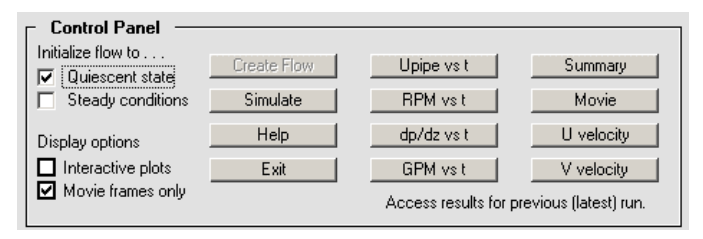


Figure 7-6d. Assuming quiescent, stagnant-flow initial conditions.

On the other hand, the fluid may be moving initially at t=0, and *then*, the transient flow specifications shown in the user interface is applied. If the initial flow is not rotating, we know that its solution does not depend on density; we can therefore calculate it assuming a very small value of ρ together with large time steps. If we wish to initialize to a non-rotating steady flow, the message box in Figure 7-6e appears, reminding the user to click "Create Flow" to start this process. Once this is completed, the "Simulate" button can be clicked to perform the required transient analysis.

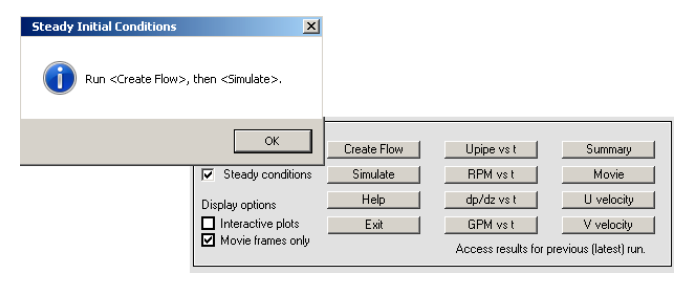


Figure 7-6e. Creating a non-rotating, steady initial flow.

If the starting flow is rotating, its solution does depend on density and time steps will need to be very small to ensure convergence. This initialization is not supported at the present time because the solution procedure cannot be made as robust or automatic as desired by the authors, but continuing research is being pursued in this area.

Example 7-7. Effect of steady rotation for power law flows in highly eccentric annuli at high densities (heavy muds).

We emphasized earlier that for non-rotating flows, the effects of density vanish at large times. Thus, in computing non-rotating steady-state flows with the transient algorithm, it is advantageous to use as small a fluid density as possible in order to quickly converge the calculations. Here we wish to evaluate the effects of mud weight under rotating conditions. For the non-Newtonian eccentric flow in Figure 7-7a, a very low specific gravity of 0.01 leads to a flow rate of 898.5 gpm. Next we wish to consider the opposite extreme, e.g., a heavy mud or cement with a specific gravity of two. Because the unstable convective term never vanishes when the pipe rotates (its magnitude is proportional to fluid density and pipe rpm), we decrease the time step to 0.0001 sec and increase the number of time steps simulated. The resulting flow rate is a much lower 135.1 gpm. Computation times for the two runs are five seconds and two minutes, approximately. Finally, we reduce the specific gravity to 1.0, i.e., an unweighted mud. Will the flow rate vary linearly with density, that is, fall midway between 135.1 and 898.5 gpm? Figure 7-7c shows that the flow rate is, in fact, 160.1 gpm. This unpredictability shows why computer models are important to real-world field job planning.

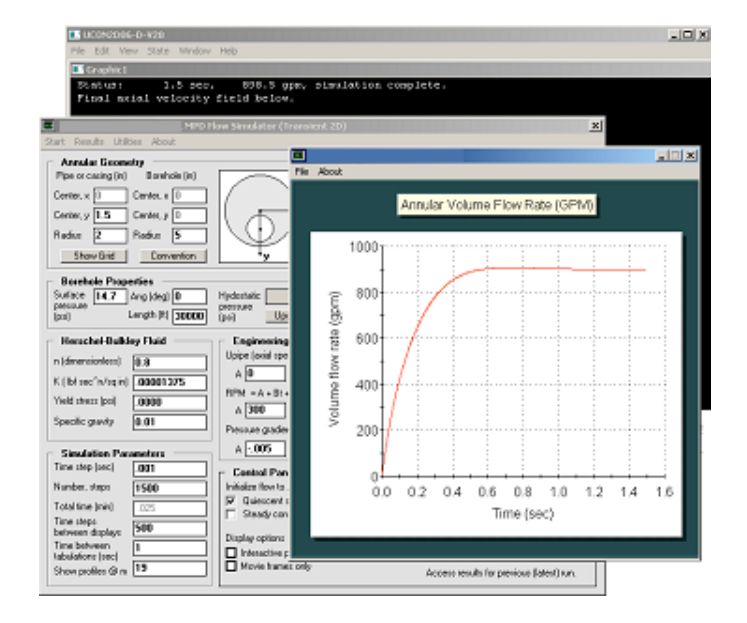


Figure 7-7a. Very low density fluid (e.g., foam) at high rpm.

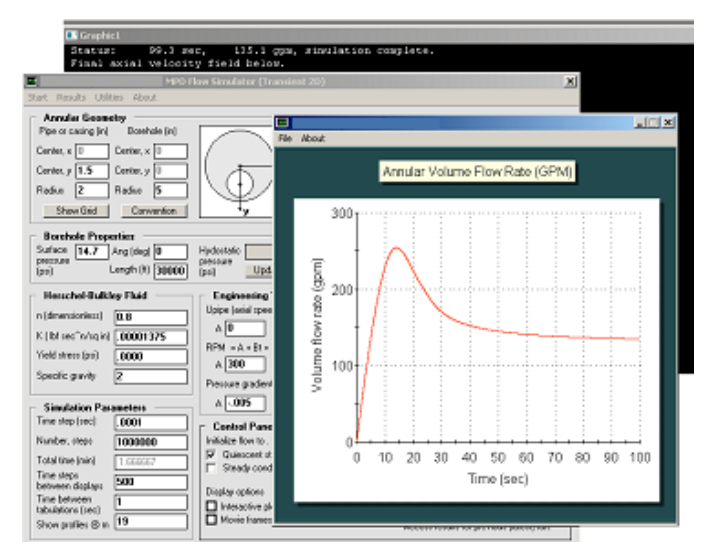


Figure 7-7b. Very high density fluid (e.g., heavy mud or cement) at high rpm.

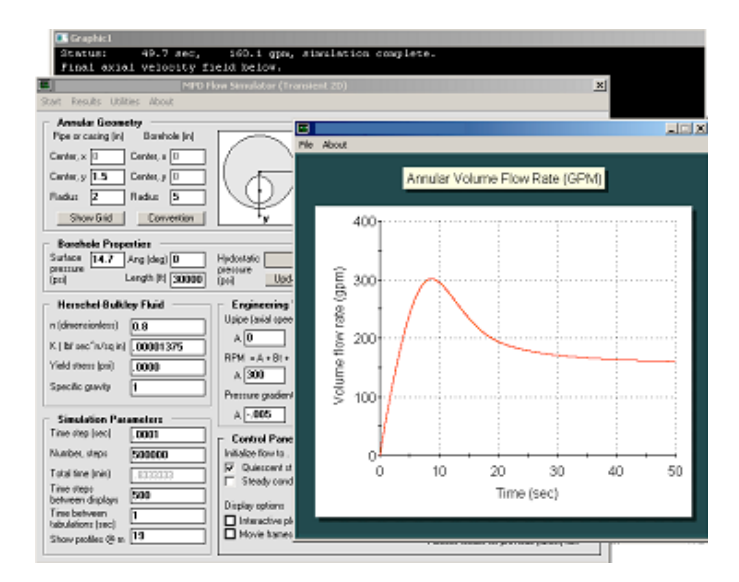


Figure 7-7c. Unweighted fluid (e.g., water or brine) at high rpm.

Example 7-8. Effect of mudpump ramp-up and ramp down flowrate under non-rotating and rotating conditions.

In Figure 7-8a, we consider a power law fluid in an eccentric annulus under a constant imposed pressure gradient of -0.005 psi/ft with the drillpipe completely stationary. This is seen to produce a steady-state flow rate of 1,051.8 gpm as shown. In practice, the mud pump starts and stops, and transient effects are associated with ramp-up and ramp-down. We ask, "How are pressure gradient and flow rate transient properties related?"

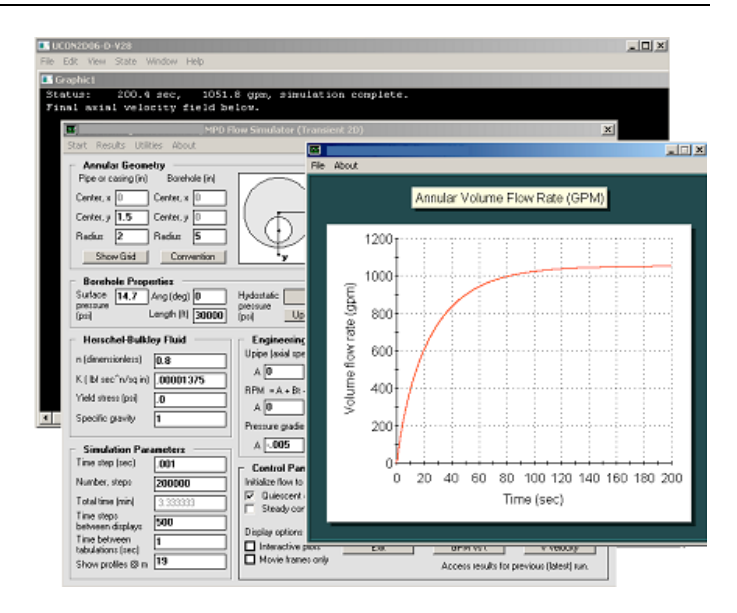


Figure 7-8a. Constant pressure gradient calculation.

To answer this question, we modify several menu entries of Figure 7-8a so that the pressure gradient is no longer constant. The assumption shown in Figure 7-8b allows a sinusoidal ramp-up from quiet conditions to the previous value of -0.005 psi/ft, followed by a full ramp-down. This is accompanied by time mesh refinement plus the use of additional time steps. Clicking on the "?" to the far right of the pressure gradient menu produces the left-side diagram of Figure 7-8c showing pressure assumptions. The right-side diagram gives the computed volume flow rate as a function of time.

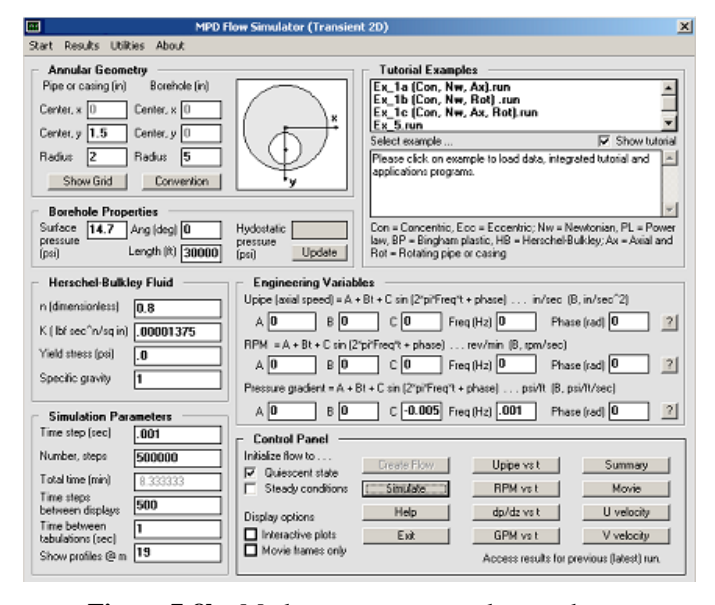


Figure 7-8b. Mudpump ramp-up and ramp-down.

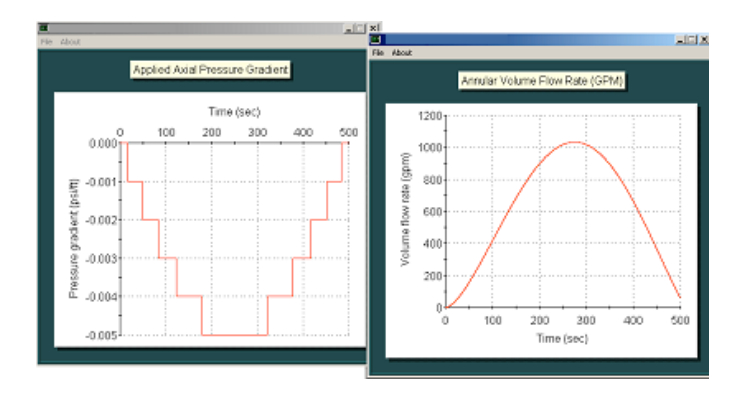


Figure 7-8c. Assumed pressure gradient and calculated flow rate.

Next, we determine the effect of drillstring rotation. We simply change the zero rotation input in Figure 7-8b to allow for a 100 rpm rotation rate as shown in Figure 7-8d. For the same pressure gradient variation as above, the flow rate is now substantially reduced as shown in Figure 7-8e.

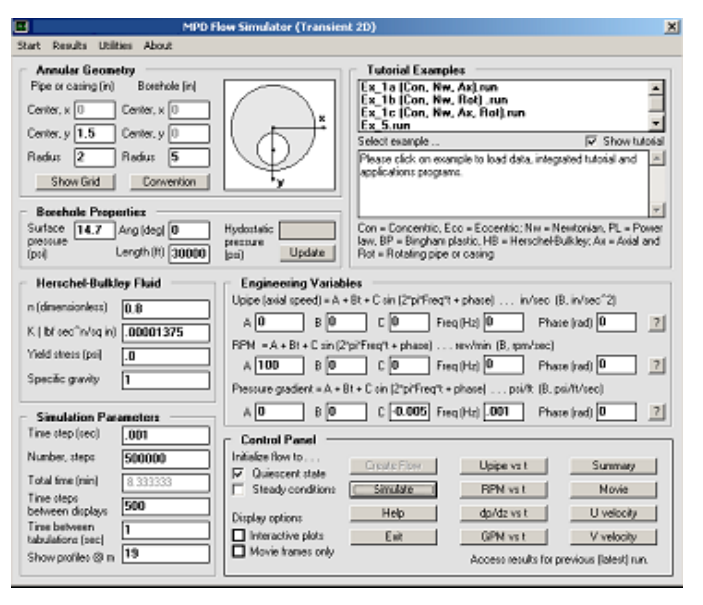


Figure 7-8d. Increasing rotation rate to 100 rpm.

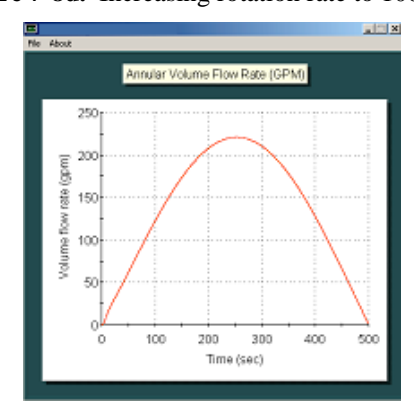


Figure 7-8e. Significantly reduced volume flow rate with rotation.

Example 7-9. Effect of rotation and azimuthal startup.

In this example, we study the effects of drillstring rotation start-up on the baseline non-rotating problem defined in Figure 7-9a for a power law fluid in an eccentric annulus. Figure 7-9b shows that after 100 sec, the (almost) steady flow rate is 1,024.0 gpm.

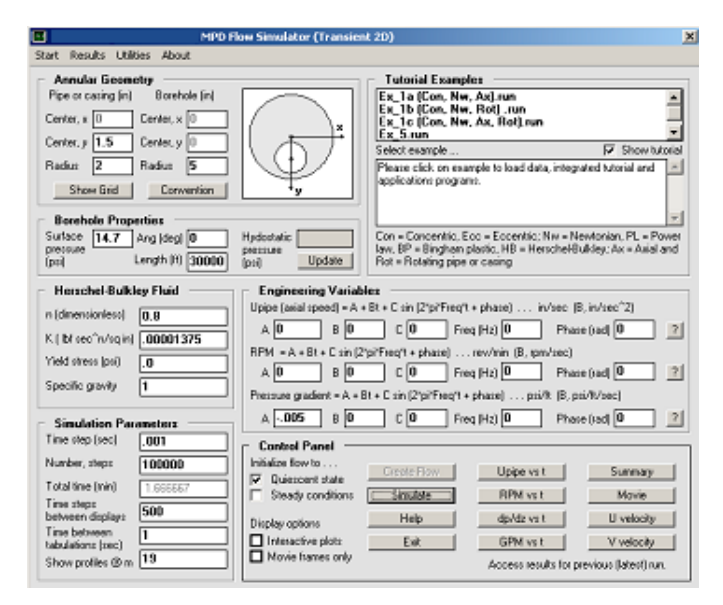


Figure 7-9a. Non-rotating flow.

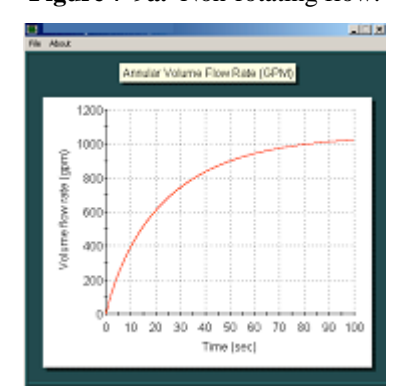


Figure 7-9b. Non-rotating flow.

What happens when the drillstring is rotating at a fixed constant 100 rpm for the duration of the start-up process? This new flow is easily obtained by changing the constant rpm input in Figure 7-9a to that in Figure 7-9c, to produce the flow rate history shown in Figure 7-9d. After 100 sec, the flow has fully equilibrated at the reduced rate 221.1 gpm. There is a flow rate "overshoot" near 350 gpm early on that we have observed on all rotational flow calculations.

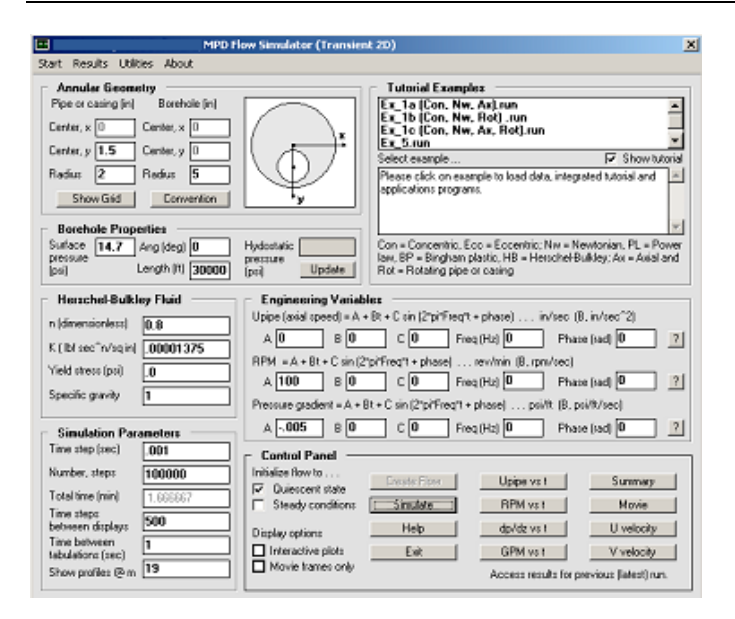


Figure 7-9c. Constant 100 rpm throughout.

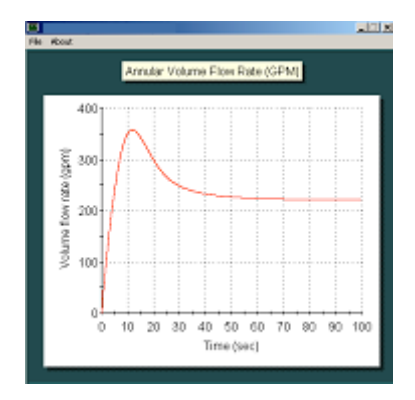


Figure 7-9d. Constant 100 rpm throughout.

We next determine the effects of rotation start-up. In Figure 7-9e, we now choose the "Bt" input option for RPM definition, typing "1" into that box for the time step information assumed. In Figure 7-9f, we show at the left how the same 100 rpm is achieved as before, but at the end of the 100 sec period. The right-side diagram shows a flow rate returning to the 200 gpm range, however, the flow rate overshoot is now near 600 gpm.

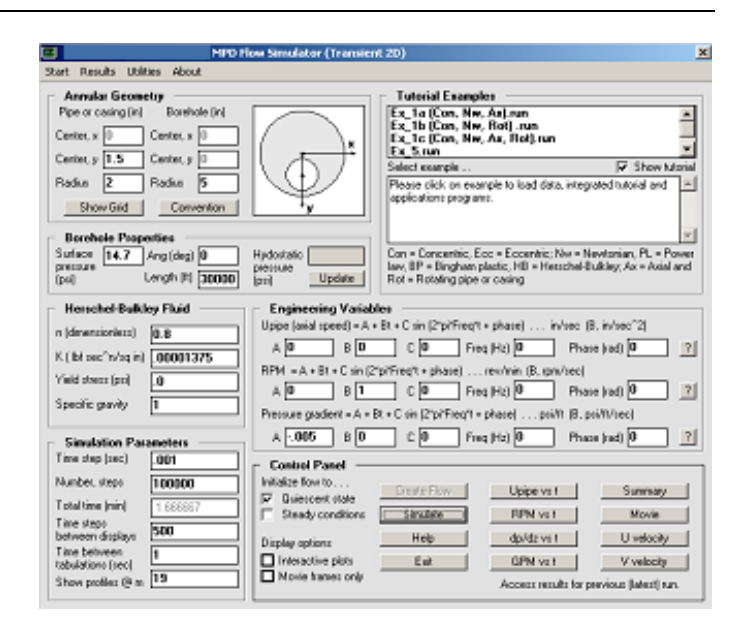


Figure 7-9e. Linearly increasing rpm with time.

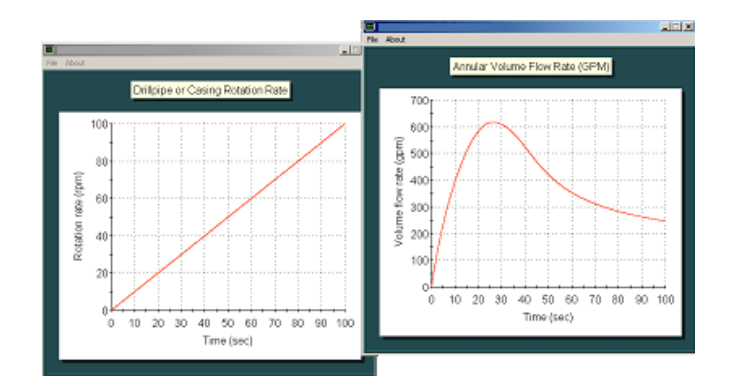


Figure 7-9f. Linearly increasing rpm with time.

Example 7-10. Effect of axial drillstring movement.

In this *non-rotating* drillstring example, we study the effects of axial movement on the baseline problem defined previously in Figure 7-9a for a power law fluid in an eccentric annulus. Again, Figure 7-9b shows that after 100 sec, the (almost) steady flow rate is 1,024.0 gpm assuming stationary pipe. If a constant +20 in/sec is modeled instead, we have an increased 1,132.6 gpm, whereas if -20 in/sec is taken, we find a reduced 912.6 gpm. Computer screens for these simple constant-speed dragging calculations are not shown.

In field applications, the drillstring is often reciprocated axially to facilitate jarring operations or cuttings removal while the mudpump acts under an almost constant pressure gradient condition. One might ask what the effects on flow rate, apparent viscosity, shear rate and viscous stress are, with the answers sure to assist the engineer in interpreting the physical consequences of his actions. For example, increases in bottomhole stress may improve hole cleaning while reductions in apparent viscosity may lubricate the drillstring. In Figure 7-10a, we alter the "U_{pipe}" input to allow sinusoidal

drillstring reciprocation with a peak-to-peak amplitude of 20 in/sec and a frequency of 0.1 Hz. Clicking on the "?" at the far right will produce the pipe displacement speed history at the left of Figure 7-10b. At the right is the stably computed oscillatory flow rate.

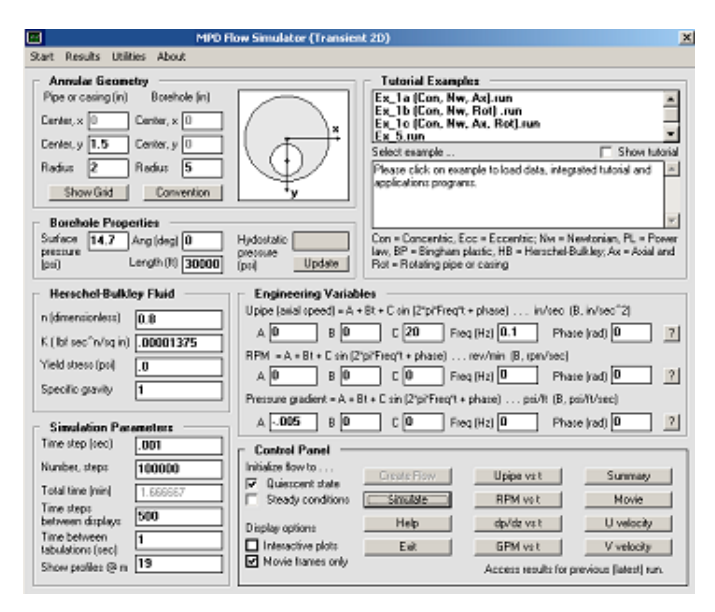


Figure 7-10a. Sinusoidal drillstring reciprocation.

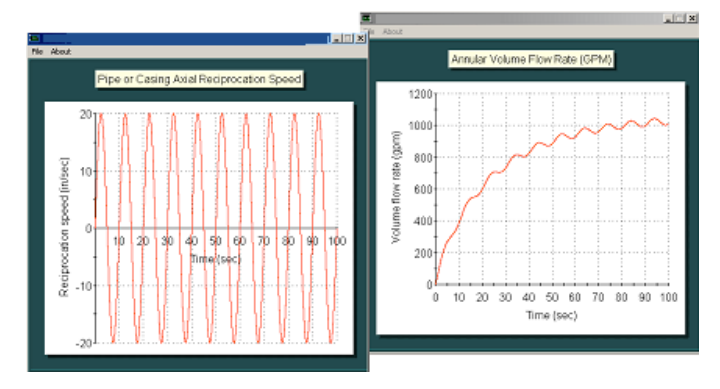


Figure 7-10b. Pipe displacement history and computed flow rate.

The "Results" menu in Figure 7-10c provides additional post-processed results useful for correlation purposes. For instance, "Color plots" provides displays of the physical quantities appearing in the list, several of which are shown in Figure 7-10d. Notice in Figure 7-10a that we had elected to save "movie frames" showing the axial velocity distribution evolving in time (the "interactive plot" option would produce line graph results during simulation). Playing the "Axial velocity – Movie" option produces a movie, which can be viewed continuously or frame-by-frame. Typical movie frames (with time increasing to the right) are shown in Figure 7-10e. All of the post-processing options described here are also available for rotating flow problems.

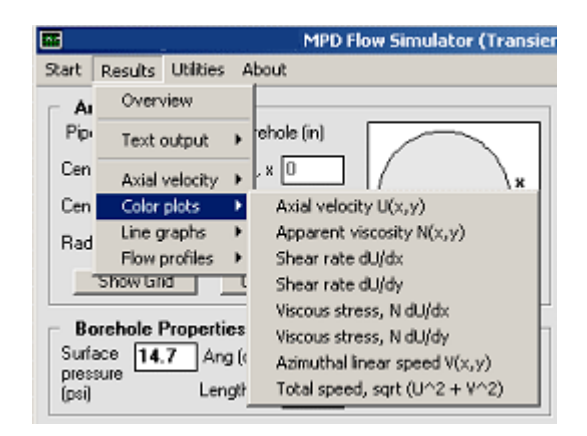


Figure 7-10c. Example color output.

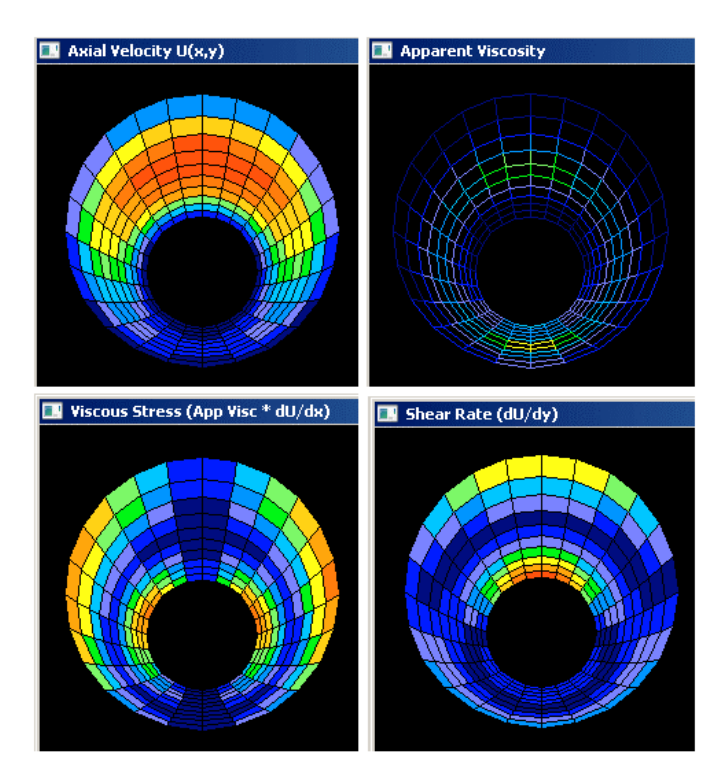


Figure 7-10d. Example color output for several physical quantities.

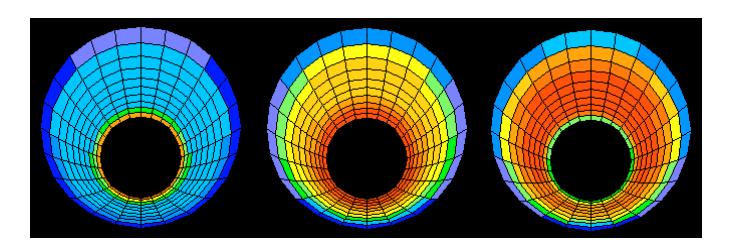


Figure 7-10e. Frames from axial velocity movie (time increasing).

Example 7-11. Combined rotation and sinusoidal reciprocation.

In this example, again for transient, nonlinear, non-Newtonian power law flow in an eccentric annulus, we combine two previous calculations and demonstrate the ease with which combined sinusoidal axially reciprocating pipe motion and drillstring rotation can be modeled, literally by filling in input boxes and clicking. The assumptions are given in Figure 7-11a, assumed pipe displacement histories are displayed in Figure 7-11b, and the computed volume flow rate is provided in Figure 7-11c. Note from this curve the pronounced overshoots and flow rate fluctuations. We have modeled the mud pump as a constant pressure gradient source in the model that leads to variable flow rate. In reality, the pump may act more as a constant rate source that leads to time-dependent pressure gradients. This latter model is much more complicated mathematically and cannot be solved within a reasonable time. However, the percent fluctuations seen from flow rate curves such as that in Figure 7-11c represent those for pressure gradient and can be used meaningfully for managed pressure job planning.

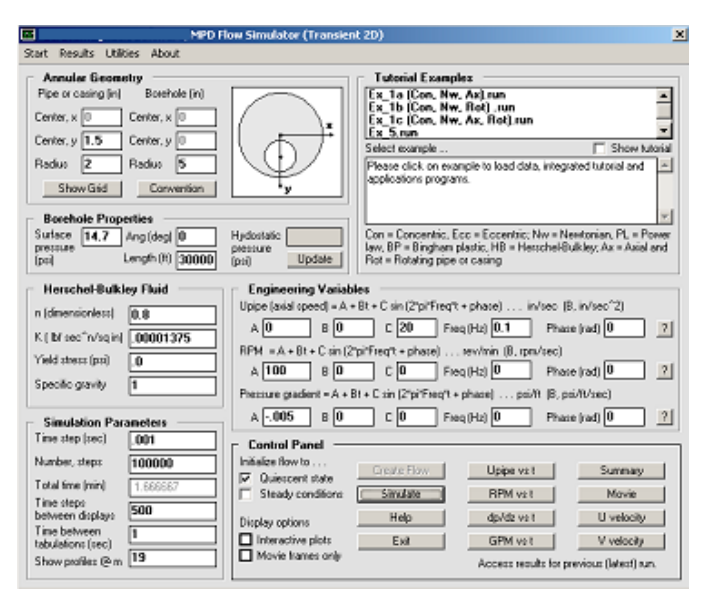


Figure 7-11a. Combined transient reciprocation and rotation.

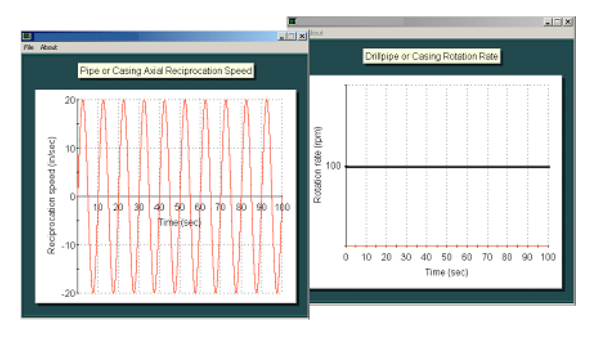


Figure 7-11b. Pipe displacement history display.

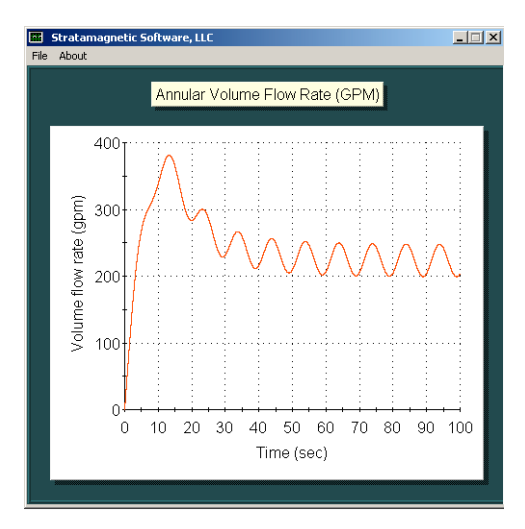


Figure 7-11c. Computed volume flow rate.

Example 7-12. Combined rotation and sinusoidal reciprocation in presence of mudpump flow rate ramp-up for yield stress fluid.

This comprehensive example illustrates the high level of simulation complexity offered by the math model. Here we again consider an eccentric annulus, however, now containing a Herschel-Bulkley yield stress fluid. The drillpipe is allowed to axially reciprocate sinusoidally in time, while rotation rate increases linearly with time. The mudpump pressure gradient is allowed to steepen with time from start-up to describe increased pumping action. All of these effects are coupled nonlinearly. They can be computed quickly and stably, and if numerical instabilities are encountered, they can be remedied by decreasing time step size. To accommodate this possibility, the algorithm is efficiently coded to make optimal use of memory resources and will allow up to 10,000,000 time steps, for which calculations may require about fifteen minutes or more. The assumptions are shown in Figure 7-12a, while detailed pipe displacement histories, applied pressure gradients and computed volume flow rate are given in Figure 7-12b.

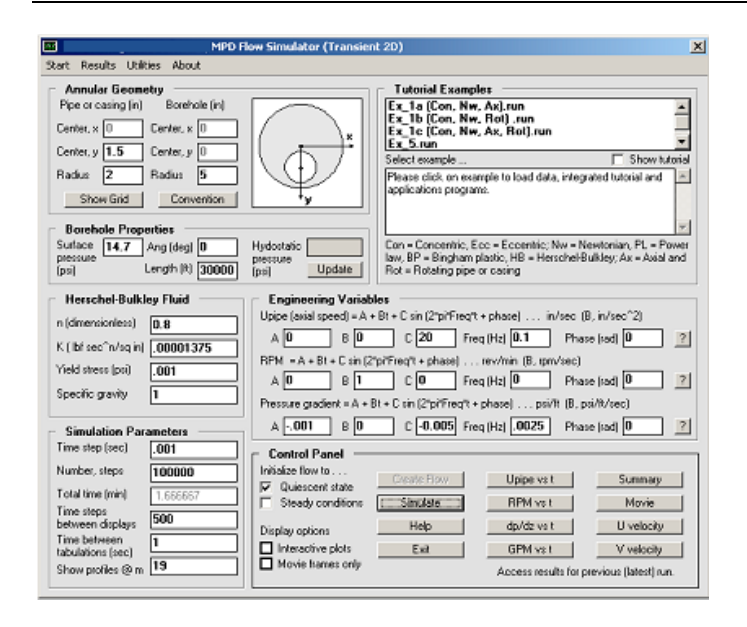


Figure 7-12a. Basic assumptions, comprehensive example.

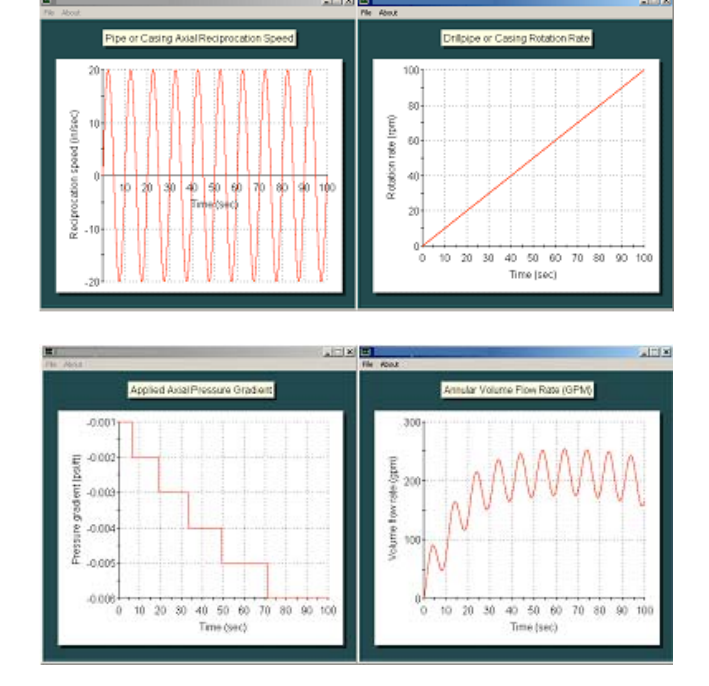


Figure 7-12b. Additional assumptions and computed flow rate with time.

Closing Remarks

The present paper describes new capabilities in modeling steady and transient non-Newtonian flow in highly eccentric annuli, with or without plug zones associated with yield stress fluids, with realistic geometric anomalies, plus effects like borehole axis curvature and drillpipe translation and rotation. The rigorous fluid-dynamical model formulated here and its exact mathematical solution, augmented by rapidly converging algorithms and convenient color displays, are intended to provide state-of-the-art capabilities useful to managed

pressure drilling, hole cleaning and cementing. The usual methods for well control include changing mud rheology, altering pump rate or schedule, and adjusting of surface choke pressure levels. We have demonstrated how pressure gradients (or, equivalently, flow rate) depends on rotation and shown how complicated operational scenarios can be modeled. This work therefore offers drillpipe rotation as an additional means for well control and drilling safety in managed pressure drilling.

Acknowledgments

The authors gratefully acknowledge 2009-2011 support from the United States Department of Energy for their technical proposal "Advanced Steady-State and Transient, Three-Dimensional, Single and Multiphase, Non-Newtonian Simulation System for Managed Pressure Drilling." effort was administered by the Research Partnership to Secure Energy for America (RPSEA) through its Ultra-Deepwater Program under Subcontract No. 08121-2502-01. curvilinear grid generation research was also supported by the United States Department of Energy, in particular, under Small Business Innovation Research Grant DE-FG03-99ER82895 in 1999-2000. We are indebted to Art Schroeder, Energy Valley, to Jim Chitwood, Chevron, and to James Pappas, RPSEA, for their encouragement and advice, and especially to John Lofton, Chevron, for his engineering insights and guidance related to several areas in the modeling of rotating pipe flow effects. The views expressed in this paper represent those of the authors only and not necessarily the opinions of any program sponsors.

References

- 1. Chin, W.C., <u>Borehole Flow Modeling in Horizontal</u>, <u>Deviated</u> and Vertical Wells, Gulf Publishing, Houston, 1992.
- Chin, W.C., <u>Computational Rheology for Pipeline and Annular Flow</u>, Elsevier, Cambridge, 2001.
- 3. Chin, W.C., Quantitative Methods in Reservoir Engineering, Elsevier, Cambridge, 2002.
- Chin, W.C. and Zhuang, X., "Exact Non-Newtonian Flow Analysis of Yield Stress Fluids in Highly Eccentric Borehole Annuli with Pipe or Casing Translation and Rotation," SPE 131234-PP, presented at the CPS/SPE International Oil & Gas Conference and Exhibition, Beijing, China, 8-10 June 2010.
- Souza Mendes, P.R. and Dutra, E.S.S., "A Viscosity Function for Viscoplastic Liquids," Annual Transactions of the Nordic Rheology Society, Vol. 12, 2004.